A. Path of the *r* Process

A nucleus of fixed Z cannot add neutrons indefinitely even in the presence of an intense neutron flux. The energy of binding of each successive neutron becomes progressively weaker as more and more neutrons are added, until ultimately the binding falls to zero. This sets an upper limit to neutron addition at fixed Z. Moreover, not even this limit will be attained because of the incidence of (γ,n) reactions at the temperature necessary to produce the neutrons by charged particle interactions. The effect of (γ,n) reactions can readily be understood from statistical considerations. Write $n(A,Z)$ and n_n for the number densities of nuclei A, Z and of neutrons respectively, and let $Q_n(A,Z)$ be the neutron binding *to* the nucleus $X(A,Z)$ in the reaction,

$$X(A,Z)+n\rightleftharpoons X(A+1,Z)+\gamma+Q_n(A,Z),$$

such that

$$Q_n(A,Z)=B_n(A+1,Z)$$
$$=c^2[M(A,Z)+M_n-M(A+1,Z)]. \quad (13)$$

Note that Q_n for nucleus A, Z is equal to the neutron binding energy B_n (taken positive) *in* nucleus $A+1$, Z. With T in units of 10^9 degrees, Q_n in Mev, and neglecting weight factors of order unity, the statistical balance in this reaction is expressed by

$$\log\frac{n(A+1,Z)}{n(A,Z)}=\log n_n-34.07-\tfrac{3}{2}\log T_9+\frac{5.04}{T_9}Q_n \quad (14)$$

with all logarithms to the base 10. For neutron addition to be highly effective we require $n(A+1,Z)/n(A,Z)\gg 1$. When $n(A+1,Z)/n(A,Z)\sim 1$, neutron addition is less effective. When $n(A+1,Z)/n(A,Z)\ll 1$, neutrons are scarcely added at all. As an approximation, adequate for the present discussion, we may consider that neutrons are added or not added according to whether $n(A+1,Z)/n(A,Z)\geq 1$ is satisfied or not, i.e., according to whether

$$Q_n\geq\frac{T_9}{5.04}(34.07+\tfrac{3}{2}\log T_9-\log n_n) \quad (15)$$

is satisfied or not. With $T_9\sim 1$ and $n_n\sim 10^{24}$ as found in Sec. III F, we have

$$Q_n\gtrsim 2 \text{ Mev}.$$

Larger Q_n values would be required at higher temperatures or at lower neutron densities. $n(A+1,Z)/n(A,Z)$ is very sensitive to small changes in Q_n or T_9. Under the conditions discussed above $5.04Q_n/T_9\approx 10$. Hence a ten percent change in Q_n, namely by 0.2 Mev, or a ten percent change in T_9, namely by 10^8 degrees, will change $n(A+1,Z)/N(A,Z)$, by a factor of ten. Conversely, for given Q_n, T_9, and Z the distribution in abundance will exhibit a sharp peak where $n(A+1,Z)=n(A,Z)$. This peak will be at most two or three units in A in width.

We have said that Q_n decreases as more and more neutrons are added at fixed Z. This statement ignored neutron pairing effects. Thus Q_n is higher for odd $N=A-Z$ by 1.5 to 3 Mev (depending on A) than it is for even $N=A-Z$. This means that instead of a simple monotonic decrease of Q_n with increasing A (Z fixed) we have two decreasing sequences, one for N odd, the other for N even, the two sequences being separated by about 2 Mev in the range of A of interest in this discussion.

Consider the effect of these two sequences on the criterion for neutron addition. Evidently the pairing effect makes it substantially more difficult for Q_n to satisfy the criterion when N is even, and hence neutron addition must always be expected to cease when N is even. Thus if a neutron can be added at N even, then a further neutron will always be added, since an additional energy approximately equal to 2 Mev is then available for binding the second neutron. On the other hand, when a neutron is added at odd N, the situation is reversed—a second neutron would in that case be less strongly bound by $\sim$2 Mev—so that, although the first neutron might satisfy our criterion, the second is a good deal less likely to do so, and eventually, when N becomes large enough, will not in fact do so. Thus we expect that neutron addition will always cease with N at an even value, so that if A is odd Z must be odd, and if A is even Z must be even.

These remarks all refer to a fixed value of Z. Now Z must increase by unity from time to time, since the neutron-rich nuclei at present under consideration are all unstable against negative beta decay, the lifetimes being $\sim$0.01–10 sec. When Z thus increases, the energy of binding of the next neutron increases quite substantially, so that one or more neutrons can again be added. Once again, however, neutron addition will cease at some even N. Neutron addition cannot then proceed until Z increases by a further unit—and so on. We therefore obtain a clear picture of how the nuclei evolve, by repeated neutron addition interspersed with β^- processes, the nuclei always being obliged to "wait" for a β^- process when neutron addition decreases Q_n to the limit allowed by our criterion. The process is shown schematically in Fig. V,2. A detail of this figure for $118<A<132$ is shown in Fig. V,3.

The *s* and *r* processes differ in a very crucial way. In the *s* process, neutrons are made available very slowly so that the neutron density is always low. In such circumstances the addition of neutrons to the nuclei is controlled by their (n,γ) cross sections. That is to say, the various nuclei compete among themselves for the capture of a slow trickle of neutrons, the abundances of the nuclei being governed by the flow equation (11)

$$dn(A)/dt=-\lambda_n(A)n(A)+\lambda_n(A-1)n(A-1),$$

where $n(A)$ is the abundance of that beta-stable isobar at A which occurs in the *s*-process capture path. In the *r* process, on the other hand, we are concerned with a

situation in which there is no neutron shortage, and neutron addition is limited not by (n,γ) cross sections but by (γ,n) competition and by "waiting" for β^- processes to take place. Essentially, we assume that equilibrium is reached between the rapid (n,γ) and (γ,n) processes, *viz.*, $n, \gamma \rightleftharpoons \gamma, n$, and that the slow beta-decay processes constitute a slow leakage from this equilibrium. The corresponding flow equation in the r process, derived from the general equation (10), takes the form

$$dn(Z)/dt = -\lambda_\beta(Z)n(Z) + \lambda_\beta(Z-1)n(Z-1), \quad (16)$$

where $n(Z)$ is the density of that isotope of element Z at which waiting for negative beta decay occurs, i.e., the isotope for which $Q_n \sim 2$ Mev. The quantity $\lambda_\beta(Z)$ is related to the beta-decay mean lifetime, τ_β, and half-life, t_β, by $\lambda_\beta = 1/\tau_\beta = 0.693/t_\beta$. The condition for steady flow in the r process is

$$\lambda_\beta(Z)n(Z) = \lambda_\beta(Z-1)n(Z-1) = \text{const}$$

or

$$n(Z) \propto \lambda_\beta^{-1}(Z) = \tau_\beta(Z).$$

This is the analog of the steady-flow condition in the s process, namely,

$$\lambda_n(A)n(A) = \lambda_n(A-1)n(A-1) = \text{const}$$

or

$$n(A) \propto \lambda_n^{-1}(A).$$

Just as the abundances of the s nuclei suggest that steady flow has occurred in the s process, so the abundances of the r nuclei suggest that steady flow has occurred in the r process.

The $n(Z)$ given by the flow equations cannot immediately be interpreted as atomic abundances. At first sight it might seem as if only certain values of A are concerned in the r process, namely the values of A at which the nuclei "wait." In Figs. V,2 or V,3, if nuclei of charge Z wait at A, nuclei of charge $Z+1$ wait at $A+\Delta A$, where ΔA equals the number of neutron captures at $Z+1$ after beta decay at Z. Thus it might appear that only atomic weights A, $A+\Delta A$, etc., are likely to be produced in any appreciable abundances by the r process. This would be the case if there were a unique track of the kind shown in Figs. V,2 and V,3. But this is scarcely likely to be the case, since there will certainly be a spread in A, Z values about this path, simply due to the statistical nature of Eq. (14). Thus a small scatter in the values of atomic weights at which waiting for beta decay occurs is only to be expected. This suggests that we convert the n_Z abundances to n_A abundances by

$$n(A) = n(Z)(\Delta A)^{-1} = n(Z)(dZ/dA), \quad (17)$$

where ΔA is the number of unit steps in A for a single step in Z along the typical track of the form shown in Fig. V,2, and dZ/dA is the slope of the track in the Z, A plane. That is to say, we "spread" the abundances accumulated at the "waiting points" over the intervals of A that occur between the waiting points. This treatment is of course approximate, but it is thought adequate for the present purpose, since the present analysis contains other simplifications that are explained at a later stage. We arbitrarily take the spread from a given waiting point at A to the next higher waiting point at $A+\Delta A$ rather than in the reverse direction. Physically, this corresponds to the assumption that, in freezing, the material accumulated at a waiting point with given A, Z is spread out, as γ radiation dies out, by final neutron captures over an interval in A up to the waiting A for $Z+1$. The equation for the equilibrium between (n,γ) and (γ,n) reactions is much more sensitive to T, (linear dependence), than to n_n, (logarithmic dependence). Thus, as T and n_n decrease, the equilibrium is displaced toward slightly greater A values, representing the capture of the last neutrons.

The solution of the dynamical problem in the r process falls into two parts. The first part consists in a determination of the track shown schematically in Fig. V,2, the second consists in estimating the beta-decay waiting time. The relative abundances given by steady flow then follow immediately from

$$n(A) \propto \frac{\tau_\beta(A,Z)}{\Delta A} = \tau_\beta(A,Z)\frac{dZ}{dA},$$

where $\tau_\beta(A,Z)$ is now the mean beta-decay lifetime at the waiting point, A, for a given Z. A determination of the track demands a precise specification of the criterion for neutron addition. This criterion can be written as $Q_n \geq Q_o$, where Q_o is to be a specified quantity, of order 2 Mev, which depends on n_n, T in accordance with the inequality (15).

The problem of the determination of the track is that of obtaining Q_n as a function of A, Z from nuclear data. Assuming for the moment this to be done, we then have $Q_n(A,Z) \geq Q_o$ as the condition for neutron addition. We now wish to determine the waiting values of A for various Z by using the following criteria.

With Z specified, $N = A - Z$ must be even, and

$$Q_n(A,Z) \geq Q_o,$$
$$Q_n(A+2,Z) < Q_o.$$

In this way the waiting points A, $A+\Delta A$, $\cdots$ corresponding to Z, $Z+1$, $\cdots$ can be found. A further necessary condition is that the waiting points increase monotonically with Z.

We have not found it possible to determine the waiting points solely from the current empirical nuclear data on neutron binding energies. This is to be expected, if it is recalled that one must know the binding energy of the very neutron-rich nuclei along the neutron capture path with considerable precision ($\sim$0.2 Mev) in order to specify the path precisely. Even the binding energies of the stable nuclei on which careful mass measurements have been made are rarely known to this

precision. Furthermore, the extrapolation to the neutron-rich nuclei involves considerable uncertainty. For these reasons we have been forced to resort to a method of calculating r-process abundances which establishes a few parameters semiempirically on the basis of certain salient features of the abundance curve itself. We now outline a method of calculation which may eventually be capable of yielding a theoretical abundance curve on the basis of nuclear data alone.

First, we consider the determination of $Q(A,Z)$ on the basis of the smooth Weizsäcker atomic mass formula (We35), neglecting shell, pairing and quadrupole deformation effects:

$$M(A,Z)=(A-Z)M_n+ZM_H-\frac{1}{c^2}\left[\alpha A-\beta\frac{(A-2Z)^2}{A}-\gamma A^{\frac{2}{3}}-\epsilon\frac{Z(Z-1)}{A^{\frac{1}{3}}}\right], \quad (18)$$

where M_n and M_H are the masses of the neutron and of the hydrogen atom and α, β, γ, and ϵ are constants in energy units, to be determined empirically. They represent, respectively, volume, isotopic, surface, and Coulomb energy parameters. In the following discussion we use $\alpha=15.3$, $\beta=22.6$, $\gamma=16.7$, and $\epsilon=0.69$, all in Mev, as determined by Fowler, Hornyak, and Cohen (Fo47). Equation (18) can be alternatively written as

$$M(A,Z)=M_A+\frac{1}{2c^2}B_A(Z-Z_A)^2, \quad (18a)$$

where

$$Z_A\simeq\tfrac{1}{2}A\left(1+\frac{\epsilon}{4\beta}A^{\frac{2}{3}}\right)^{-1} \quad (19)$$

is the value of Z at a given mass number, A, for which $M(A,Z)$ has the minimum value, M_A. Z_A is not necessarily integral, and both M_A and Z_A can be determined in terms of the empirical constants by setting $\partial M/\partial Z=0$, keeping A constant. The coefficient B_A appears in the well-known parabolic dependence of $M(A,Z)$ on Z and can be evaluated from

$$B_A=\frac{8\beta}{A}\left[1+\frac{\epsilon}{4\beta}A^{\frac{2}{3}}\right]\simeq\frac{4\beta}{Z_A}. \quad (20)$$

Alternatively, M_A, Z_A, and B_A can be taken as quantities to be determined as empirical functions of A.

Returning to Eq. (18), we can determine $Q_n(A,Z)$ as follows

$$\begin{aligned}Q_n(A,Z)&=c^2[M_n+M(A,Z)-M(A+1,Z)]\\&=\alpha-\beta\left(1-4\frac{Z^2}{A^2}\right)-\tfrac{2}{3}\gamma A^{-\frac{1}{3}}+\frac{\epsilon}{3}\frac{Z(Z-1)}{A^{\frac{4}{3}}}\\&\simeq\alpha-\beta-\tfrac{2}{3}\gamma A^{-\frac{1}{3}}+4\beta\frac{Z^2}{A^2}\left[1+\frac{\epsilon}{12\beta}A^{\frac{2}{3}}\right].\end{aligned} \quad (21)$$

The terms in the second line in Eq. (21) can be identified successively as due to volume, isotopic, surface, and Coulomb effects in atomic masses. Equating Q_n to a specified Q_o in Eq. (21) gives A as a smooth function of Z. The plot of Z against A runs approximately parallel to the stability line, but it is depressed below this line by an amount that depends on the value of Q_o. For $Q_o=2$ Mev the depression amounts to about 7 units in Z at $A\sim100$ and about 11 units in Z at $A\sim200$. If the nuclear masses were really given by the Weizsäcker formula the nuclei would evolve along this line, not completely in a smooth fashion because of the discrete nature of A, but smoothly within one unit of A. There would be no gross deflections of the line, such as are implied in Figs. V,2 and V,3. In addition, the values of τ_β and dZ/dA would also be a smooth function of A, so that the theory would be incapable of explaining the peaks and troughs of the abundance curve for the r nuclei. Evidently an improved expression must be used for $M(A,Z)$ if the theory is to provide this degree of detail. We have not attempted a complete treatment but have been content to approximate in a degree that does not seem to have too serious an impact on the calculated results. A fuller treatment of the form of $M(A,Z)$ is at present being investigated by Dr. Forrest Mozer at the California Institute of Technology, and improved results should be forthcoming from its use.

Our treatment is based on modifying the above expression for $M(A,Z)$ so that we have

$$M(A,Z)=M_W(A,Z)-\frac{1}{c^2}[f(N)+g(Z)], \quad (22)$$

where $M_W(A,Z)$ represents the Weizsäcker expressions given in Eq. (18). That is to say, we subtract a sum of two functions, one of the neutron number and the other of the proton number. Insofar as they are functions of N and Z separately, this procedure takes into account the important effects on nuclear masses of (i) neutron or proton shell structure, (ii) spheroidal quadrupole deformation of partially filled shells, and (iii) pairing of neutrons and pairing of protons. Products of two such functions are not included. The quantities $f(N)$ and $g(Z)$ will be discontinuous functions at magic closed shell numbers for N or Z respectively. The sign is taken negative so that $f(N)$ and $g(Z)$, as positive quantities, decrease the mass and add to the stability of a nucleus.

We now obtain

$$Q_n(A,Z)=\alpha-\beta-\tfrac{2}{3}\gamma A^{-\frac{1}{3}}+4\beta\frac{Z^2}{A^2}\left[1+\frac{\epsilon}{12\beta}A^{\frac{2}{3}}\right]+f'(A-Z), \quad (23)$$

where

$$f'(A-Z)=f'(N)=\frac{df(N)}{dN}=f(A+1-Z)-f(A-Z).$$

Note that $g(Z)$ drops out of Q_n. Care must be exercised in evaluating f' at magic numbers where f is discontinuous. Our criterion $Q_n \geq Q_o$, with Q_o a specified number ~ 2 Mev, now gives a track in the Z, A plane that depends on $f'(A-Z)$.

The capture path is changed considerably on taking $f'(A-Z)$ into account. The plot of Z against A for the r process follows a smooth curve approximately parallel to the stability line if the Weizsäcker mass formula, Eq. (18), is used. The plot of Z against A, shown in Fig. V,2, departs from such a smooth curve, however. Deviations are introduced by the function $f(A-Z)$. Most notably, this function causes the curve to swing upwards towards the stability line whenever $A-Z$ equals a neutron magic number. The physical reason for this is that the energy of binding of the next neutron decreases sharply by about 2 Mev at neutron shell closure. Consider neutron shell closure at $N=A-Z=82$, $A=123$, $Z=41$ (cf. Fig. V,3). The 82nd neutron is added with a binding of 2 Mev, or perhaps somewhat more than this, the value of Z being some 12 units below the stability line at this stage. An 83rd neutron cannot then be added at such a depth below the stability line because of the sharp fall of binding after shell closure. Indeed, an 83rd neutron at $Z=41$ would scarcely be bound at all. Further evolution then depends on a β^- process, which decreases $A-Z$ to 81. An 82nd neutron can then be added, but an 83rd again cannot. A further β^- process must therefore take place, when once again an 82nd neutron can be added. In this way the nucleus climbs a staircase with Z and A both increasing by unity at each step. Eventually, however, the climb up the staircase carries the nucleus close enough to the stability line for an 83rd neutron to be added at a binding energy ~ 2 Mev. This occurs for $Z=49$, $A=131$. Subsequently Z increases by one unit, not for a one-unit increase of A, as on the staircase, but for an increase of some three or more units in A. The differential in A must be an odd integer since waiting occurs only for even N. We refer to the values of A and Z for a magic N at which more than one capture occurs as the "break-through" values at the abundance peaks. Break-through pairs are (82, 32), (131, 49), and (196, 70) at $N=50$, 82, and 126, respectively, and staircases similar to the one at $N=82$ occur at $N=50$ and 126. These staircases are associated with the rising sides of major peaks in the abundance curve for the r process. More subtle effects of proton shells and spheroidal deformations are discussed later.

From the above discussion it would seem that the capture path cannot be determined without explicit knowledge of $f(A-Z)$, but this is not so, as the following device shows. Let A_e, Z_e be a nucleus with empirically known neutron-binding energy, and with

$$N_e = A_e - Z_e = A - Z = N.$$

Then we have

$$Q_n(A_e,Z_e) = \alpha - \beta - \tfrac{2}{3}\gamma A_e^{-\frac{1}{3}} + 4\beta\frac{Z_e^2}{A_e^2}\left[1+\frac{\epsilon}{12\beta}A_e^{\frac{2}{3}}\right] + f'(A_e - Z_e), \quad (23a)$$

where

$$f'(A_e - Z_e) = f'(A-Z).$$

Subtracting Eq. (23a) from (23), we have

$$Q_n(A,Z) = Q_n(A_e,Z_e) + \tfrac{2}{3}\gamma(A_e^{-\frac{1}{3}} - A^{-\frac{1}{3}}) + 4\beta\frac{Z^2}{A^2}\left[1+\frac{\epsilon}{4\beta}A^{\frac{2}{3}}\right] - 4\beta\frac{Z_e^2}{A_e^2}\left[1+\frac{\epsilon}{4\beta}A_e^{\frac{2}{3}}\right]$$

$$\simeq Q_n(A_e,Z_e) - 4\beta\left[\frac{Z_e^2}{A_e^2} - \frac{Z^2}{A^2}\right] - 0.4. \quad (24)$$

In the last approximate expression we have evaluated in Mev the differences in the surface and Coulomb terms for the cases which will be found to be of interest. The isotopic term in β is by far the largest term in the difference in neutron binding energy for two nuclei with the same N. The important result of the foregoing analysis is that $g(Z)$ does not appear in (23) for $Q_n(A,Z)$ and $f(N)$ and $f'(N)$ do not appear in (24). This follows from our assumptions that to first order the deviations from the Weizsäcker mass law are separable in N and Z.

If the values of $Q(A_e,Z_e)$ were always accurately known the present procedure would be simple of application. Unfortunately, individual empirical values of $Q(A_e,Z_e)$ contain sufficient inaccuracies to cause serious difficulties if employed singly. The difficulties can be overcome, in part, by a suitable form of smoothing, except for values of $A-Z$ between ~ 84 and ~ 110, in which range the empirical mass data seem to be too poorly known even to admit of smoothing.

Smoothing is effected by constructing the quantity

$$\Delta\langle f'(A_e - Z_e)\rangle_{\text{Av}} \simeq \Delta\left[Q_n(A_e,Z_e) - 4\beta\frac{Z_e^2}{A_e^2}\right]_{\text{Av}}.$$

The quantity in square brackets is first calculated for each nucleus for which empirical values of Q_n are available, and then averaged over all cases having the specified value of $N=A_e-Z_e$. The Δ indicates that the values are calculated relative to those at the beginning of the appropriate neutron shell. Thus $\Delta\langle f'\rangle$ is the excess neutron binding energy *to* nuclei with a specified N over that given by the smooth Weizsäcker mass formula normalized to zero at the beginning of the shell in which N lies. We have used the nuclear mass tables of Wapstra (Wa55) and Huizenga (Hu55) for this purpose. When this has been done for various N the resulting average values have been plotted against N, as in Fig. VII,1. A second form of averaging is then effected by drawing a smooth curve through the points obtained in this way, values being finally read off the curve.

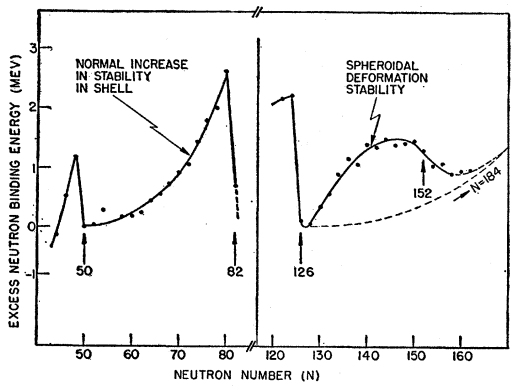

FIG. VII,1. The average excess neutron binding energy *to* nuclei with neutron number N, over that given by the smooth Weizsäcker atomic mass formula (We35). Each value has been normalized to the value at the beginning of the shell in which N lies. Empirical mass data for the $N=82$ to 126 shell are not accurate enough to yield the portion of the curve in this region.

We interpret the "quadratic" rise in the neutron binding excess between $N=50$ and 82 as the normal behavior as a neutron shell is filled. The last neutrons interact with a greater number of nucleons and are bound by about 2.6 Mev more than the first neutrons in this shell. In the $N=126$ to 184 shell there is a rapid rise to great stability early in the shell, a flattening off, and eventually a decrease having a maximum slope near $N=152$. We assume that eventually the curve rises again to a high value at shell closure. The early rise may be attributed to the ability of these heavy nuclei to take up spheroidally deformed shapes which have lower energy levels for extra neutrons than the spherical shape at the beginning of the shell. Maximum deformation is reached apparently near $A\sim144$ and then the shell becomes spherical again on closure, with the normal shell effect coming into play. The effect of spheroidal deformations on quadrupole moments and on rotational level structure in heavy nuclei has been brilliantly developed by Bohr and Mottelson (Bo53) and extensive calculations of energy levels in spheroidal potentials have been made by Nilsson (Ni55). Nuclei in the $N=51$ to 82 shell do not show these effects in a pronounced manner, and thus "normal" shell behavior can be expected. The effects are well known in the heavier $N=82$ to 126 shell, for which, unfortunately, masses accurate enough for our purposes are not available. The effects can be expected to be highly developed in the $N=126$ to 184 shell. The influence of the enhanced stability on the r process is discussed in detail in what follows. *Note added in proof.*—The recent mass spectroscopic data of W. H. Johnson, Jr., and V. B. Bhanot (Jo57) yield a curve in the range $N=82$ to 126 similar to the right-hand curve in Fig. VII,1.

A difficulty which arises in determining the $Q_n(A,Z)$ from the empirical $Q_n(A_e,Z_e)$ lies in the isotopic parameter β for which we have taken the value 22.6 Mev. This is the value which gives the correct dependence of Z_A on A if the Coulomb coefficient ϵ is taken as 0.69 Mev. Fowler *et al.* (Fo47) found this value for ϵ to be necessary to fit the rise of the packing fraction curve for nuclei with $A>70$, and Green has confirmed this point (Gr54b). This value for ϵ is somewhat larger than that found in early attempts to adjust the smooth Weizsäcker formula to nuclear masses but is in keeping with the smaller values of nuclear radii found in electron scattering experiments by Hofstadter and his collaborators (Ho56c). However, in determining $Q_n(A,Z)$ from $Q_n(A_eZ_e)$ we really need "local" values of β at $N=A-Z=A_e-Z_e$, not the average value determined by the best fit to Z_A over all A. This implies that β is not constant, as is indeed found to be the case if one adjusts the Weizsäcker formula or its alternative form in M_A, B_A, Z_A to local regions. Unfortunately, the empirical values for $Q_n(A_e,Z_e)$ do not cover a sufficient spread in A_e and Z_e to give accurate determinations of the local values for β, and thus the extrapolation to A,Z values far from the stability line involves considerable uncertainty.

To elaborate, let us consider the accuracy with which we must compute Q_n for the waiting point, A, at a given Z value along the capture path not near any magic

TABLE VII,1. Parameters of the r process at magic neutron numbers.

N	A	Z	Process	Q_n[a] Mev	Z_A	B_A Mev	$\frac{1}{2}\delta_A$ Mev	W_β Mev	τ_β sec	A	n(calc)	n(obs)
50	80	30	$(\beta^-\nu_-)$	1.9	35.0	1.90	1.43	3.82	12.3	1	42.6	33.8
	81	31	$(\beta^-\nu_-)$	2.4	35.4	1.88	···	4.07	8.96	3	10.4	6.62
	82	32	(n,γ)	2.9[a]				Break-through point				
82	128	46	$(\beta^-\nu_-)$	1.0	54.5	1.36	1.18	7.48	0.43	1	Stan.	1.48
	129	47	$(\beta^-\nu_-)$	1.4	54.9	1.36	···	7.84	0.34	1	1.17	1.05
	130	48	$(\beta^-\nu_-)$	1.7	55.3	1.35	1.16	5.82	1.50	3	1.73	···
	131	49	(n,γ)	2.0[a]				Break-through point				
126	194	68	$(\beta^-\nu_-)$	1.2	77.9	1.16	0.77	8.31	0.25	1	0.87	0.533
	195	69	$(\beta^-\nu_-)$	1.4	78.3	1.16	···	8.39	0.24	3	0.28	0.548
	196	70	(n,γ)	1.6[a]				Break-through point				

[a] The values for Q_n, at which (n,γ) occurs at the recognizable break-through points of the magic-neutron-number peaks in the atomic abundance curve, have been used to establish a smooth dependence of Q_n on atomic weight.

shell number in N. We evaluate

$$\left.\frac{\partial Q_n}{\partial A}\right|_Z \simeq -\frac{8\beta Z^2}{A^3} \sim -0.25 \text{ to } -0.1 \text{ Mev},$$

where the numerical values have been determined near $A=100$ and $A=200$, respectively. Since the Q_n can hardly be specified to better than 0.5 Mev an uncertainty in A of several units is to be expected. The break-through points near magic shell numbers for N can be evaluated from

$$\left.\frac{\partial Q_n}{\partial A}\right|_N \simeq +\frac{8\beta ZN}{A^3} \sim 0.5,\ 0.3,\ 0.2 \text{ Mev},$$

where the numerical values have been determined at $N=50$, 82, 126, respectively. Again an uncertainty of one or more units in A arises from uncertain knowledge of the Q_n.

With these difficulties in mind, we have chosen to establish a few key points in the track of the r process by using the values for the atomic weights at those peaks in the atomic abundance curve which are attributed to the r process. On the leading edges of these peaks there is no arbitrariness, except in the value of A (or Z) at which a given magic N is reached, and in the value of A (or Z) at which break-through occurs. The break-through points at which neutron capture without a preceding beta decay becomes possible occur just beyond the maxima of the magic-neutron-number abundance peaks. We have chosen these break-through points to give the best fit to the three abundance peaks due to magic neutron-numbers and have then adjusted the path determined by our criterion $Q_n(A,Z)\geq Q_0$ to fit the three points and to give a smooth run of waiting points between these break-through points. Thus the r-process path has been determined by a smooth curve for Q_0 passing through the break-through values at $N=50$, 82, and 126. These key values are shown in Table VII,1, where we list the Q_n values calculated by the smoothing procedures, using $\beta=22.6$ Mev. These Q_n values show a systematic decrease from 2.9 Mev at $N=50$, through 2.1 Mev at $N=82$ to 1.6 Mev at $N=126$. These values correspond to temperatures of 1.45, 1.0, and 0.8×10^9 degrees, respectively, for $n_n=10^{24}$. Whether or not this systematic decrease is real is a matter which cannot be answered with present knowledge of nuclear masses and binding energies. In attempting to use estimated local values for β we have found that the differences in Q_n and thus T are only accentuated. It is clear that the conditions, n_n and T, for the production of the three peaks were not greatly different. A small difference, if real, would be very significant in our understanding of the astrophysical circumstances under which the r-process elements were synthesized. We return to this matter later in our discussion and in Sec. XII. The capture path from Fe^{56} to $A=265$ which we have used is given in Table VII,2 and is illustrated in Figs. V,2 and V,3. The path is complete except for a gap from $A=150$ to $A=185$, in which region the empirical masses are so poorly known that there is no guide at all even to the trend of the capture track.

TABLE VII,2. The path of the r process and calculations of r-process abundances.

N	A	Z	Z_A	B_A Mev	$\frac{1}{2}\delta_A$ Mev	W_β Mev	τ_β sec	ΔA	Atomic abundances
30	56	26	...	...	...	...	...	...	Starting point
42	68	26	30.3	2.40	1.40	3.42	21.4	3	First waiting point
44	71	27	31.4	2.20	...	4.68	4.45	7	2.20
50	78	28	34.2	1.94	1.42	6.26	1.04	1	3.61
	79	29	34.6	1.92	...	6.45	0.90	1	3.11
	80	30	35.0	1.90	1.43	3.82	12.3	1	42.6
	81	31	35.4	1.88	...	4.07	8.96	3	10.4
52	84	32	37.4	1.80	1.44	4.28	6.96	1	24.2
	85	33	37.8	1.78	...	4.59	4.91	5	3.40
56	90	34	39.8	1.70	1.44	4.67	4.50	7	2.23
62	97	35	42.5	1.60	...	8.50	0.225	5	0.156
66	102	36	44.5	1.55	1.41	8.39	0.241	5	0.167
70	107	37	46.5	1.50	...	11.00	0.062	3	0.072
72	110	38	47.7	1.47	1.35	9.73	0.115	7	0.057
78	117	39	50.5	1.41	...	13.19	0.025	3	0.029
80	120	40	51.7	1.39	1.27	12.02	0.040	3	0.046
82	123	41	52.8	1.38	...	13.33	0.024	1	0.083
	124	42	53.1	1.37	1.23	11.05	0.061	1	0.211
	125	43	53.5	1.37	...	11.46	0.051	1	0.176
	126	44	53.8	1.37	1.20	9.30	0.144	1	0.500
	127	45	54.2	1.36	...	9.61	0.122	1	0.423
	128	46	54.5	1.36	1.18	7.48	0.427	1	1.48
	129	47	54.9	1.36	...	7.84	0.338	1	1.17
	130	48	55.3	1.35	1.16	5.82	1.50	3	1.73
84	133	49	57.6	1.33	...	8.61	0.211	3	0.244
86	136	50	57.6	1.31	1.08	6.10	1.18	9	0.454
94	145	51	60.6	1.28	...	9.59	0.123	5	0.085
126	185	59	74.9	1.18	...	16.31	0.009	1	0.030
	186	60	75.3	1.18	0.78	14.82	0.014	1	0.049
	187	61	75.6	1.18	...	14.78	0.014	1	0.049
	188	62	75.9	1.17	0.78	13.06	0.026	1	0.091
	189	63	76.3	1.17	...	13.14	0.025	1	0.088
	190	64	76.6	1.17	0.78	11.54	0.049	1	0.170
	191	65	76.9	1.16	...	11.40	0.052	1	0.180
	192	66	77.3	1.16	0.77	9.94	0.103	1	0.357
	193	67	77.6	1.16	...	9.90	0.105	1	0.364
	194	68	77.9	1.16	0.77	8.31	0.252	1	0.874
126	195	69	78.3	1.16	...	8.39	0.240	3	0.278
128	198	70	80.4	1.16	0.76	8.90	0.180	11	0.056
138	209	71	83.9	1.16	...	12.56	0.032	3	0.037
140	212	72	84.9	1.16	0.75	11.81	0.043	3	0.050
142	215	73	86.0	1.16	...	12.68	0.030	3	0.035
144	218	74	87.0	1.16	0.75	11.93	0.041	3	0.048
146	221	75	88.1	1.16	...	12.80	0.029	3	0.034
148	224	76	89.1	1.16	0.74	12.06	0.039	3	0.045
150	227	77	90.2	1.16	...	12.91	0.028	3	0.032
152	230	78	91.3	1.16	0.73	12.30	0.036	1	0.123
	231	79	91.6	1.16	...	12.22	0.037	1	0.127
	232	80	91.9	1.16	0.73	10.67	0.072	3	0.084
154	235	81	93.0	1.16	...	11.52	0.049	3	0.057
156	238	82	93.4	1.16	0.72	10.10	0.095	3	0.110
158	241	83	94.5	1.16	...	10.94	0.064	1	0.221
158	242	84	94.8	1.16	0.72	9.41	0.136	3	0.157
160	245	85	95.9	1.16	...	10.24	0.089	3	0.103
162	248	86	97.0	1.16	0.72	9.64	0.120	3	0.139
164	251	87	98.0	1.16	...	10.36	0.084	3	0.097
166	254	88	99.0	1.16	0.72	9.64	0.120	3	0.139
168	257	89	100.1	1.16	...	10.48	0.029	3	0.091
170	260	90	101.2	1.16	0.71	9.87	0.107	5	0.074[a]
174	265	91	102.9	1.16	...	11.40	0.052	7	0.026[a]

[a] Probably depleted by neutron-induced fission.

B. Calculation of r-Process Abundances

We now pass to the conclusion of our problem, namely, calculation of the relative abundances of the elements produced in the r process. This involves determination of $\Delta A=\partial Z/\partial A$ and τ_β at the waiting points. The capture path calculated from the criterion $Q_n(A,Z)\geq Q_o$ yielded nonintegral values of Z and A and thus a fairly smooth $\partial Z/\partial A$ along the track which we used as a guide as discussed above. In the track we

have finally chosen in Table VII,2, and in the "actual" track, Z and A change by integral values, and so we have chosen to use the integral ΔA listed in Table VII,2, in calculating $n(A)$. In Table VII,2 the various parameters needed in the abundance calculations are also listed.

The mean beta-decay lifetimes at the waiting points have been calculated from the Fermi expression

$$\tau_\beta = \frac{1}{\lambda_\beta} = \frac{10^4}{W_\beta{}^5} \text{ sec},$$

where W_β, measured in Mev, is the effective beta-decay energy at the waiting point. It includes the kinetic energy of the electron and neutrino and the rest-mass equivalent energy (0.5 Mev) of the electron. The numerical constant has been determined by using an allowed transition $\log_{10} ft$ value of 3.85, where

$$f = \frac{1}{30}\left[\frac{W_\beta}{m_o c^2}\right]^5 \simeq W_\beta{}^5$$

if W_β is measured in Mev, and $t = 0.693\tau_\beta$ is the beta-decay half-life. The method described below for evaluating W_β leads in general to an underestimate, so that our values of τ_β could be too large by a factor of as much as 10. However, the relative values and thus the relative abundances should not be uncertain by such a large factor.

The determination of W_β as a function of the waiting point charge, Z, and mass, A, is a matter of some complexity. The total kinetic energy, Q_β, available in the beta transition to the ground state of the daughter nucleus is calculable from the atomic mass expression given in Eq. (22) and becomes

$$Q_\beta = c^2[M(A,Z,N) - M(A, Z+1, N-1)].$$

Since the masses are atomic rather than nuclear, no allowance need be made for the beta-electron mass. We thus have,

$$Q_\beta = B_A(Z_A - Z - 0.5) + \frac{dg}{dZ} - \frac{df}{dN}. \qquad (25)$$

In this expression dg/dZ and df/dN explicitly appear. However, since they appear as a difference their influence on Q_β cannot be too great. Except at shell numbers, g and f increase with Z and N, respectively. If g and f were linear in Z and N with the same coefficient, then $dg/dZ - df/dN$ would be zero. Actually, g and f are approximately quadratic in the nuclear excess over magic-number values. Since there is a neutron excess in negative beta decay, in general $df/dN > dg/dZ$ and Z_A and B_A are usually smaller than the values calculated from the smooth formula. Z_A changes discontinuously at magic numbers, increasing after N magic and decreasing at Z magic. Actually, the residual effect of these terms can be taken into account by using just the first term of Eq. (25) for Q_β with local values for B_A and Z_A, particularly for Z_A. Local values for Z_A have been given by Coryell (Co53) and we have used these values as tabulated in Table VII,2. Z_A is not only a function of A but also of the shell in which Z and N fall. Coryell chose the smooth Weizsäcker relation between local values of B_A and Z_A, namely $B_A Z_A \simeq 4\beta$, but we have not found this to be sufficiently accurate for our purpose. Accordingly, we made an independent analysis in order to obtain the values of B_A listed in Table VII,2. To do this we used Coryell's Z_A at a given A and determined B_A from the empirical Q_β differences calculable at a given A from the masses of Wapstra (Wa55) and Huizenga (Hu55). These values of B_A are shown as a function of A in Fig. VII,2.

We thus have

$$Q_\beta = B_A(Z_A - Z - 0.5),$$

where B_A and Z_A are now the "local" values for these quantities taking into account all deviations from the Weizsäcker mass law except odd-even effects, which must be treated separately, as discussed below, for nuclei with odd A and even A. It is emphasized that Z_A must be chosen to correspond to the shells in which Z and N lie.

The beta-ray transition to the ground state of the daughter nucleus will rarely be allowed. Allowed transitions occur to excited states of the daughter nucleus having spins differing by zero or unity from those of the parent ground state and having the same parity. Of these allowed transitions perhaps one is favored by a large matrix element indicating considerable similarity in the initial and final states as to spin, isobaric spin, and orbital characteristics. The excitation of this favored state will in general be lower at larger A, since the level density increases with A. It can be argued that the amount of excitation ought to be proportional to, and of the order of magnitude of, the isobaric parameter B_A. We have arbitrarily chosen $2B_A$ as the excitation energy of the excited state to which the beta transition effectively occurs. With this choice, the relative heights of the abundance peaks at $N = 50$, 82, and 126 are approximately reproduced as indicated by a comparison of the columns giving n(obs) and n(calc) in Table VII,1. The choice of $2B_A$ probably errs on the high side, so that our estimates for W_β may be somewhat low.

We can now write down W_β as soon as pairing energy or odd-even terms are clarified. If δ_A is used to designate the pairing energy term, and if odd A nuclei are taken as arbitrary standards for which no pairing correction is made, then for the mass of the ground states of even A, even Z, even N nuclei we must subtract $\delta_A/2$, and for even A, odd Z, odd N nuclei we must add $\delta_A/2$. Our waiting nuclei all have even N, so that for odd A no correction is necessary and for even A we must subtract $\delta_A/2$. On the other hand, the special symmetry properties of the ground states of nuclei insofar as pairing

effects are concerned do not apply to the excited states. This has been shown by Hurwitz and Bethe (Hu51) in connection with their analysis of the neutron capture cross section of odd A and even A nuclei. Hence, we neglect pairing energy terms in the daughter nuclei. As a final result, then,

$$W_\beta = B_A(Z_A - Z - 2.5) + 0.5 \begin{cases} +0 & A \text{ odd, } Z \text{ odd} \\ -\frac{1}{2}\delta_A & A \text{ even, } Z \text{ even.} \end{cases}$$

This prescription leads if anything to an underestimate of W_β, as indicated above, so that our values for $\tau_\beta \sim W_\beta^{-5}$ may be high by as much as a factor of ten. The term $m_0c^2 = 0.5$ Mev has been added to give the total kinetic plus rest mass energy of the effective beta decay. For $\delta_A/2$ we use the empirical values tabulated by Coryell (Co53). His values of $\delta_A/2$ as a function of A are shown in Fig. VII,2. The resulting values of W_β are given in column 7 of Table VII,2 and have been used to calculate the values of τ_β given in column 8. These in turn have been used to calculate the abundances given in column 10, arbitrarily taking the abundance of ${}_{52}Te_{76}^{128}$ near the $N=82$ peak as standard at 1.48 on the Suess and Urey scale. The calculated abundances are shown as a histogram for comparison with Suess and Urey abundances which are plotted as points in Fig. VII,3. The results of the calculations, extended into the range above $A=209$, are shown in Fig. VII,4.

From Fig. VII,3 reasonable but not exact agreement with observed abundances is obtained on the basis of the theory of the r process that has been outlined. The

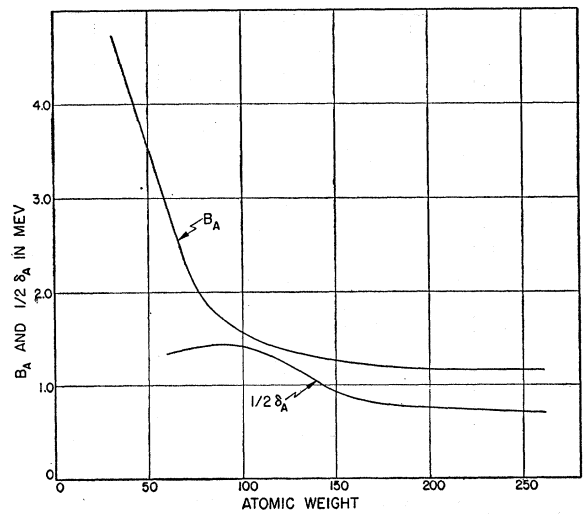

FIG. VII,2. The parameters B_A and $\delta_A/2$ as a function of atomic weight. B_A was calculated by the method described in the text, while $\delta_A/2$ is taken from the work of Coryell (Co53).

break-through values for A were established from the rounding-off points of the three observed abundance peaks ascribed to $N=50$, 82, and 126, respectively. However, the rapid rise in abundance below the peak point is unambiguously given by the rapid decrease in beta-ray energy as the track is held in the Z, A plane to the magic N numbers until break-through is finally attained. The relative abundances of the peaks come out quite well on our calculations, but this can be attributed to our arbitrary choice of the excitation energy, $2B_A$,

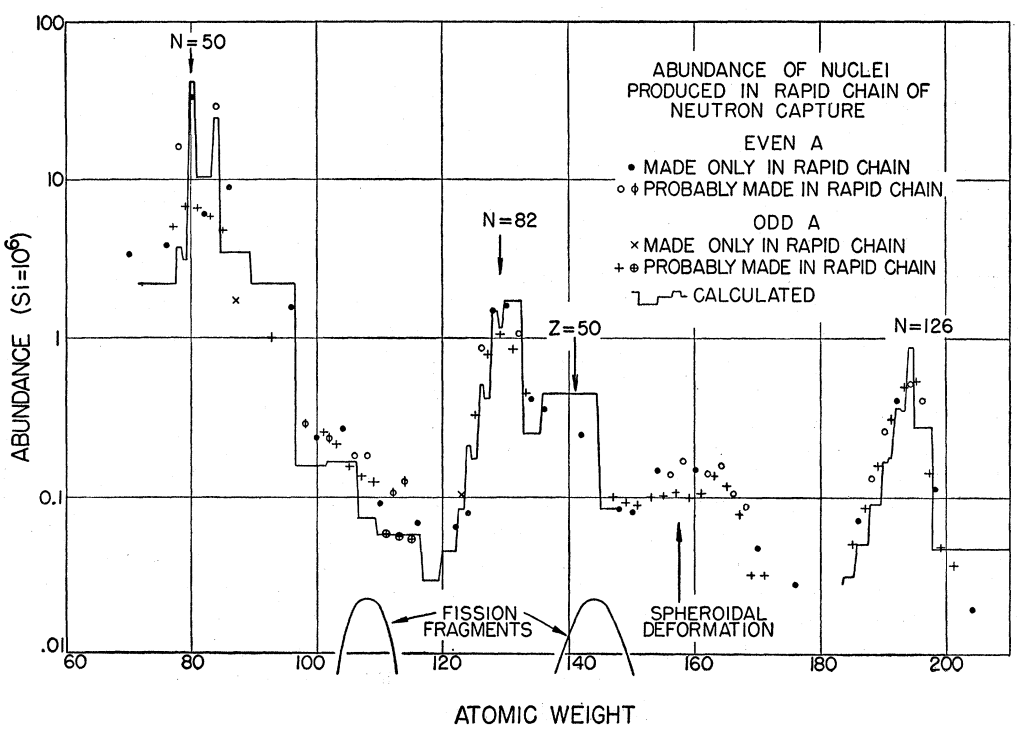

FIG. VII,3. Abundances of nuclei produced in the r process. The empirical points are taken from Suess and Urey (Su56). The histogram is a curve calculated by the methods described in the text. The free parameters have been adjusted to yield the correct relative heights of the three abundance peaks for magic neutron numbers $N=50$, 82, and 126.

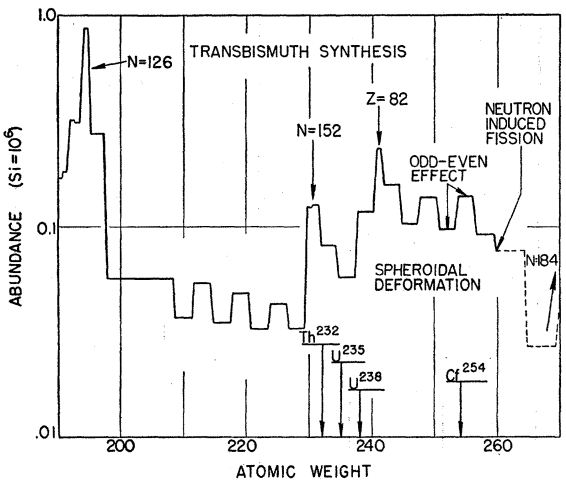

FIG. VII,4. Abundances of heavy nuclei produced in the r process. The method of calculation was the same as that used in calculating the abundance histogram shown in Fig. VII,3. It is assumed that neutron-induced fission terminates the r process at $A=260$.

in the residual nucleus after beta decay. We can conclude as follows: on the basis of the r-process track shown in Fig. V,2 which passes through neutron-rich nuclei with neutron-binding energies of the order of 2 Mev, and on the basis of beta-decay lifetimes for these nuclei computed from reasonable local values for the parameters B_A, Z_A, and $\delta_A/2$, it has been possible to compute a satisfactory caricature of the abundances of those nuclei which have been produced predominantly in the r process.

Let us discuss a few special features of the calculated histogram of Fig. VII,3. In the first place, the $N=50$ peak is really a double peak with maxima at $A=80$ and $A=84$. The empirical validity of this double peaking rests on the ratios $Se^{80}/Se^{82}=33.8/5.98$ and $Kr^{83}/Kr^{84}/Kr^{86}=5.89/29.3/8.94$, determined by the mass spectroscope. Changing the Se/Kr ratio, which might be possible in view of the divergent methods of obtaining their individual abundances, does not lead to a solution of the problem. It is also difficult to question the assignment of these isotopes to the r process. This situation can be caricatured in the r process by (i) letting $A=80$, $Z=30$ be the last nucleus at $N=50$ for which beta decay is followed by only one neutron capture; (ii) letting break-through occur at $A=81$, $Z=31$, with beta decay followed by three neutron captures to $A=84$, $Z=32$, $N=52$; (iii) making this last described nucleus a waiting point followed by only one neutron capture, in keeping with the empirical fact that the binding energy of the 53rd neutron is as small as that of the 51st neutron. Beyond this point the abundance curve trails off gradually as the neutron binding energy for increasing N gradually increases up to $N=82$ and the capture process slowly returns to the off-peak path.

The backside of the $N=126$ peak is very precipitous, in keeping with the fact that the neutron-binding energy rapidly increases after the drop at $N=126$, and the rapid return to the very neutron-rich nuclei gives a small dZ/dA ($dN/dA\sim1$), a small τ_β, and hence a small abundance. As noted previously, the rapid increase in neutron-binding energy after $N=126$ can be attributed to the fact that the first neutrons in the $N=127$ to $N=184$ shell can distort the closed nucleon shells ($N=126$, $Z=82$) in such a way as to lead to a spheroidal deformation considerably more stable than the spherical shape at the end of the preceding shell. When maximum deformation is reached, further neutron addition does not lead to greater stability, and the neutron-binding energy curve reaches a plateau. This results in the r-process path moving somewhat closer to the stability line in the Z, A plane. This leads in turn to somewhat greater values of τ_β and dZ/dA and thus to a moderate increase in abundance. It is to this spheroidal deformation effect that we attribute the abundance hump from $A=230$ to 260 in Fig. VII,4. Additional discussion of this feature is given in Sec. VIII. We also attribute the abundance hump near $A=160$, which is evident in Fig. VII,3, to this same effect, even though we have not been able to make detailed calculations in this region. It is well known that the stable nuclei in this region show large quadrupole moments consistent with the fact that the most stable forms of the ground states are spheroidal rather than spherical in shape.

The precipitous drop expected on the backside of the $N=82$ peak is masked by the appearance of a peak due to the magic number of protons, $Z=50$. It might be thought that in a neutron capture process, proton magic numbers would be irrelevant. However, a proton magic number does affect the beta-decay lifetime by slowing down the transition to the nucleus containing a proton outside the closed shell. Another way of expressing this is to note that, for example, Z_A does not increase when Z changes from 49 to 50 in Table VII,2, and thus W_β decreases, τ_β increases, and the abundance hump evident at $A=140$ in Fig. VII,3 is to be expected. Since dZ/dA becomes quite small at Z magic, as numerous neutrons are added before decay to the proton in the next shell occurs, we find that the abundance value established at the waiting point ($A=136$) is spread out over a considerable interval of atomic weights up to $A=145$.

C. Time for the r Process: Steady Flow and Cycling

The r-process abundances have been calculated on the assumption that a steady state is reached in which the abundances are proportional to the beta-decay lifetimes at the waiting points. The circumstances under which the steady state is a good approximation can be elucidated by considering the individual beta decay times and total time for the r process. From Table VII,2 Fe^{56}, taken as the source nucleus, rapidly captures some 12 neutrons to produce Fe^{68}, the first waiting point in

the "typical" capture path. Here Q_n is less than Q_o ($\sim$3 Mev in this region) for the first time and beta decay occurs with a lifetime of $\sim$21 sec. This is longer than all the succeeding lifetimes and is in fact $\sim$25% of the total time for the r process. This latter quantity is just the sum of all the τ_β in Table VII,2, plus a rough estimate of 3 sec for the region $A=150$ to 185, and is therefore $\sim$80 sec. After passing Fe^{68}, the material spends $\sim$40 sec in the $N=50$ (and 52) peak. Thus the long-lived "source" and first "sink" control the flow for a considerable period during which the heavier, shorter-lived products come into, and remain in equilibrium with, these long-lived predecessors. It is significant that the Fe^{68} lifetime plus the $N=50$ peak lifetime is long as compared with the 5 to 23 sec lifetimes of Mg^{22}, Na^{21}, etc., which control the production of the neutrons. It is also significant that the total time for the r process is comparable to the $\sim$100-sec expansion and cooling time for the supernova envelope.

From the correspondence of the calculated abundances with those in the atomic abundance distribution, it would seem that this distribution was produced under conditions in which steady flow was just reached and maintained. Other conditions can pertain in different circumstances. The establishment of steady flow requires about 38 neutrons per capturing Fe^{56}, since the average atomic weight in the distribution given in Fig. VII,3 is $\simeq$94. For fewer than 38 neutrons per Fe^{56}, the upper end of the abundance curve will not reach its full value. For a greater number of neutrons, as will certainly be the case in some supernovae, the abundances of high atomic weight will be enhanced over those illustrated in Fig. VII,3. This enhancement occurs over the entire region above $A\sim110$ because of cycling resulting from the neutron-induced fission process near $A\sim260$. For asymmetric fission, one-half of the flow is returned near $A\sim110$ and the full flow is maintained above $A\sim150$. Thus the abundances above $A\sim110$ grow relative to those below $\sim$110, with a factor of two marking the growth above $A\sim150$ relative to that for $A\sim110$ to 150. For a neutron to iron-group abundance ratio $\gtrsim100$, practically all of the original "seed" nuclei will be cycling in the region $A\sim110$ to 260 and increasing in abundance with average atomic weight $A\simeq174$. Under these circumstances the peaks at $N=82$ and $N=126$ have about the same abundances, since only one half of the material is returned to the $N=82$ peak in the cycling. In Sec. XII we consider the case of enhanced production above $A\sim110$ to be typical for certain supernovae.

D. Freezing of the r-Process Abundances

Implicit in our comparison of calculated abundances with those observed is the assumption that the unstable nuclei produced at mass number A in the r process subsequently decay only by beta decay to their stable isobars with the same mass number. This is indeed the predominant final step in the synthesis of a stable nucleus by the r process as the temperature and neutron flux decrease and the r process abundances are "frozen in." In some cases beta decay can occur to a state of the residual nucleus in the final chain of beta decays which is so highly excited that it is unstable to neutron emission. This is similar to the delayed emission of neutrons following fission. Since this mode of decay is not the main one, we have neglected it in our calculations. We note here, however, that delayed neutron emission occurs for even-even nuclei, since the depression of their ground states results in the availability of higher excited states when they are produced. Thus, this process favors odd A production over even A, since some even A mass chains switch to odd by delayed neutron emission. This point tends to compensate for the fact that even A abundances are somewhat greater than odd A abundances before the freezing occurs.

Smart (Sm48, Sm49) suggested, in connection with primordial synthesis of the elements, that (γ,n) reactions compete with negative beta decay in the freezing after a rapid neutron capture process. In this way the shielded isobars could be produced. In stellar synthesis the shielded isobars are produced separately in a second process which we have labeled the s process and which we suggest has occurred during the giant stage of stellar evolution. It is our belief that (γ,n) reactions subsequent to the r process, primordially or in supernovae, cannot have produced the shielded isobar abundances found in the atomic abundance curve.

It has been noted in Sec. VI that the barium isotope ratios and absolute abundances are consistent with p- and s-process production. Let us now consider the difficulties arising in an attempt to explain the observed barium abundances, for example, on the basis of (γ,n) reactions in the freezing of the r process. In the first place the possibility can be considered that the neutron flux suddenly ceases while the temperature is still high and that (γ,n) reactions rather than negative beta decays return the material to the stability line. This would require the ejection of some 10 to 30 neutrons per product nucleus and would obviously be self-defeating in that it would almost restore the original neutron flux. Furthermore it would invalidate the explanation for the r-process peak abundances given in this section and would require double abundance humps to have been produced in the r-process path near $A\sim100$, 140, and 200, for which there are no known reasons.

A more reasonable possibility is that suggested by Smart; after the original very fast beta decays bring the nuclei close to the stability line, the beta lifetimes become long and the (γ,n) process competes in the final adjustments. Thus in the case of barium, material produced at A just greater than 138 might stop, after fast beta decay, in the long-lived unstable barium isotopes ${}_{56}Ba_{83}^{139}$ (85 min), ${}_{56}Ba_{84}^{140}$ (12.8 days), and ${}_{56}Ba_{85}^{141}$ (18 min). Then (γ,n) processes would scour out the

loosely bound 85th, 84th, and 83rd neutrons and pile up the material in $_{56}Ba_{82}^{138}$ with its tightly bound 82nd neutron. Some leakage to the lighter isotopes could occur and a general tailing off in abundance from $_{56}Ba_{82}^{138}$ to $_{56}Ba_{74}^{130}$ would be expected. This is indeed found with the important exception that $_{56}Ba_{74}^{130}$ is even slightly more abundant than $_{56}Ba_{76}^{132}$, which is not to be expected at all. Furthermore, if the (γ,n) process does occur at barium, why does it not occur for xenon? On the basis of this process one would expect magic $_{54}Xe_{82}^{136}$ to be the most abundant of the xenon isotopes, with a tailing off to $_{54}Xe_{70}^{124}$. This is not found to be the case. $_{54}Xe_{78}^{132}$ is the most abundant isotope of xenon and is 2 to 3 times as abundant as $_{54}Xe_{80}^{134}$ and $_{54}Xe_{82}^{136}$. On the other hand, this is just what is to be expected if it is supposed that the *s* and *r* processes are operating separately. $_{54}Xe_{78}^{132}$ is the heaviest stable isotope of xenon which can be produced in the *s* process, and presumably it has the smallest (n,γ) cross section. $_{54}Xe_{80}^{134}$ and $_{54}Xe_{82}^{136}$ are made only in the *r* process, and they are low in abundance in keeping with the general ratio of the *r*-process abundances to the *s*-process abundances in this region.

Returning to the case of barium, we must finally emphasize that in the Suess and Urey distribution Ba^{138} is very abundant compared to its neighbors. If it were made by (γ,n) reactions following the *r* process, this would require an abundance peak in the primary path at A just greater than 138, for which no explanation can be given in terms of known "magic" properties. On the other hand its great production in the *s* process is understood in terms of its own magic properties.

VIII. EXTENSION AND TERMINATION OF THE *r* PROCESS AND *s* PROCESS

A. Synthesis of the Naturally Radioactive Elements

Because of its long time-scale and because it builds through the beta-stable nuclei, the *s* process is incapable of producing the naturally radioactive elements beyond bismuth. Bismuth ($Z=83$) is the heaviest of the elements with an isotope which does not decay by electron emission, alpha-particle emission, or fission. As is discussed in detail later, the short-lived alpha-emitting isotopes of polonium, which are produced after bismuth, terminate the *s* process by cycling its products back to lead.

On the other hand, just because of its short time-scale and because it builds through charge-poor, neutron-rich nuclei, the *r* process can produce transbismuth elements. These proton-poor nuclei are relatively more stable to alpha emission and fission than their stable isobars at a given A.

A convincing experimental demonstration of this was given by the production of Cf^{254} and other nuclei in the November, 1952, thermonuclear hydrogen bomb test at Bikini, as reported by Fields *et al.* (Fi56). These nuclei were synthesized by the instantaneous irradiation of U^{238} by an intense neutron flux. The successive addition of neutrons to U^{238} built U^{254} and other neutron-rich uranium isotopes. After the explosion, the U^{254} decayed rapidly to beta-stable Cf^{254}. The Cf^{254} was detected in the test debris through its spontaneous decay by the fission process. The energy release in the spontaneous fission is 220 Mev per decay, which is very large compared to the energy emitted in alpha decay ($\sim$5 Mev) or beta decay ($\sim$1 Mev). Fields *et al.* reported the half-life of Cf^{254} as 55 days. More recent measurements by Thompson and Ghiorso (Th57) yield a preliminary value of 61 days while Huizenga and Diamond (Hu57) have recently obtained a value of 56.2 ± 0.7 days.§ The Cf^{254} is unique in that it is the only beta-stable nucleus which decays predominantly by spontaneous fission with a half-life between a few days and 10^4 years.

The authors and their collaborators (Bu56, Ba56) have associated the *r* process astrophysically with the explosion of supernovae of Type I. A characteristic feature of supernovae of Type I is that after an initial period of 50–100 days the light curve exhibits an exponential decline corresponding to about 0.0137 magnitudes daily or a half-life of 55 days. The uncertainties in this half-life are discussed in Sec. XII. The close correspondence between this value and that for Cf^{254} suggested that Cf^{254} was produced in the supernova explosion along with the other products of the *r* process. Because of its large energy release per decay it was supposed in this earlier work that the Cf^{254} would dominate the radioactive energy input into the supernova debris for the order of a year after the original outburst. In the following part of this section we discuss the radioactive decay of the *r*-process products which give the radioactive energy input for Type I supernovae. The connection between the energy input and the light curve for Type I supernovae is discussed in Sec. XII. The source of the great flux of neutrons required in supernovae has been discussed in Sec. III.

B. Extension and Termination of the *r* Process

(1) *Radioactive Energy Input in Type I Supernovae*

Certain of the calculations necessary for computing the radioactive energy release by *r*-process products have been made by Schuman (Sc57a). He has analyzed the mode of decay and calculated the total decay energy for the longest-lived neutron-rich nuclei produced in each mass chain where the *r* process extends beyond the stable nuclei ($A>209$). His results, modified by new data, are incorporated in Table VIII.1. The total decay

§ The calculations which are described in this section have all been made using a half-life of Cf^{254} of 61 days, since the authors were not aware of the work of Huizenga and Diamond when they were made. Clearly, the value obtained by them is in better agreement with the original result of Baade for the half-life of the light curve of the supernova in IC 4182.

energy includes all subsequent shorter-lived activities which quickly come into equilibrium with the decay listed. Neutrino kinetic energy is not included; 45% of the energy released in each beta decay is assigned to the electrons. In addition we list in Table VIII,1 all mass chains produced in the r process below $A=209$ which beta decay with maximum half-lives in excess of 3 days. In the table all chains with maximum half-lives less than 3 days are neglected, except for the fast spontaneous fission decays at the end of the table, which are designated (SF) in column 4; (n,f) indicates neutron-induced fission.

Table VIII,1 illustrates the fact that after the rapid beta decays in a given mass chain which immediately follow the termination of an r-process event, the beta-stable nuclei above bismuth decay either by fission to the middle of the periodic table, or by alpha emission and further beta decay to the long-lived nuclei listed. Those above uranium then decay to Th^{232} ($4n$ naturally radioactive series), Np^{237} ($4n+1$ series), U^{238} ($4n+2$ series), and U^{235} ($4n+3$ series), and eventually to Pb^{208}, Bi^{209}, Pb^{206}, and Pb^{207}. *The tabulated results confirm the uniqueness of Cf^{254}. It is the only beta-stable, neutron-rich nucleus which decays predominantly by spontaneous fission with a half-life between 10 days and 10^4 years.* The table clearly indicates that the energy released by any fission decay exceeds the energy release of any alpha-plus-beta chain by a factor of five, and thus qualitatively the dominance of the radioactive energy release by Cf^{254} is assured.

It is important to consider the empirical evidence which underlies this matter of the uniqueness of Cf^{254}. Ghiorso (Gh55) has presented a graphic display of this evidence by plotting spontaneous fission and alpha-emission half-lives *versus* neutron numbers for the transuranium nuclei. Ghiorso's diagram is shown in Fig. VIII,1. The spontaneous fission half-lives decrease precipitously in value for all elements beyond the "magic" neutron number $N=152$. In what way 152 is magic, we discuss below. For $N<152$, the fission half-lives for a given Z show the characteristic rise with increasing N, to be expected from the well-understood increase in lifetime with decreasing value of the fission parameter, $Z^2/A=Z^2/(Z+N)$ (Bo39). This parameter is proportional to the ratio of the nuclear Coulomb energy to the nuclear surface energy. The alpha-emission half-lives also decrease at $N=152$, but then recover and resume their normal increase with N, since the essential nuclear bindings increase with N, while the Coulomb energy, upon which the alpha-particle decay energy is linearly dependent, remains essentially constant. The result is the sudden occurrence, within one isotope or two for each element, of spontaneous fission as the predominant mode of decay rather than alpha emission. Ghiorso's diagram, with its ordinate of some 28 factors of ten in half-life, shows that the sudden dominance of this mode of decay occurs over a wide spectrum of half-lives for the various transuranium elements.

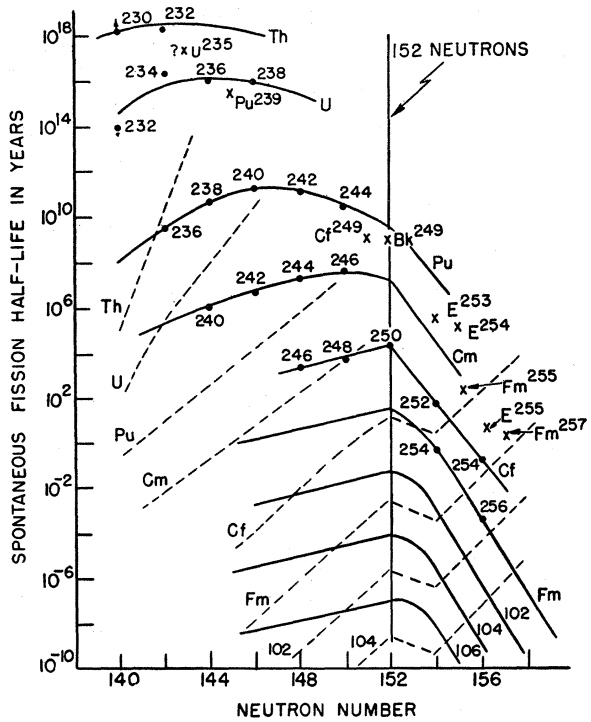

FIG. VIII,1. The analysis by Ghiorso (Gh55) of the spontaneous fission half-life (solid lines) against neutron number. Dotted lines indicate the experimentally observed alpha half-life variation except in the cases of elements 102 and 104.

Only for $_{98}Cf^{254}$ does it occur when the fission lifetime is anywhere near 55 days. For fermium it occurs at Fm^{256} with a fission lifetime of 3 hours (measured), while for curium it occurs at $_{96}Cm^{250}$ with a fission lifetime of 10^4 years (estimated). For the other relevant californium isotopes, Cf^{250} has $t_\alpha=3\times10^4$ years and $t_{SF}=10^4$ years, so that it decays by spontaneous fission a considerable proportion of the time, while Cf^{252} has $t_\alpha=2.2$ years and $t_{SF}=66$ years, so that it decays 3% of the time by spontaneous fission. For Cf^{254}, on the other hand, $t_{SF}=56$ days while $t_\alpha\geq100$ years (estimated). The fission activity predominates to the extent that alpha decay has not yet been observed for Cf^{254}.

As an empirical rule the spontaneous fission lifetime for $N\geq152$ is a function primarily of A. Thus it is 2×10^9 sec for $A=252$, 5×10^6 sec for $A=254$, 10^4 sec for $A=256$, ~10 sec for $A=258$, and $\sim10^{-3}$ sec for $A=260$.

To obtain a quantitative measure of the energy released by radioactivity by the products of the r-process event, we must multiply Schuman's calculations and those which we have made of the energy release for each mass chain, by an estimate of the relative production of the fast-decaying progenitor of that chain in the event itself. This is done in Table VIII,1, where the last columns give the total energy released, and the initial energy released measured in Mev/day. In his original calculations Schuman assumed that equal amounts of

TABLE VIII,1. Radioactive energy release of mass chains produced in the r process with half-life >3 days.

A	Element	Longest half-life, seconds, days or years	Decay type	Decay energy Q Mev	Initial abund. n_0 (Si $=10^6$)	Total energy n_0Q Mev	Initial en. rate $0.7\ n_0Q/i\mathfrak{t}$ Mev/day
3	H	12.26y	β	0.01		for reference only	
10	Be	2.7×10^6y	β	0.25		for reference only	
14	C	5600y	β	0.08		for reference only	
32	Si	~300y	β	0.82	50	40.8	$\sim1.1\times10^{-4}$
33	P	25d	β	0.12	50	5.95	0.165
35	S	87d	β	0.08	50	3.75	0.0299
39	A	260y	β	0.22	50	12.8	9.3×10^{-5}
45	Ca	160d	β	~0.11	1	~0.11	$\sim4.8\times10^{-4}$
47	Ca	4.7d	β	1.83	100	183	26.9
59	Fe	45d	β	1.36	30	40.8	0.628
60	Fe	$\sim3\times10^5y$	β	~0.05	30	~0.15	$\sim9.4\times10^{-9}$
63	Ni	80y	β	~0.03	10	~0.3	$\sim7\times10^{-6}$
79	Se	7×10^4y	β	~0.08	3.1	~0.248	$\sim6.7\times10^{-9}$
85	Kr	10.4y	β	0.31	3.4	1.05	1.9×10^{-4}
89	Sr	54d	β	0.66	3.4	2.24	0.0287
90	Sr	28y	β	1.26	2.2	2.77	1.9×10^{-4}
91	Y	58d	β	0.70	2.2	1.54	0.0183
93	Zr	9×10^5y	β	~0.03	2.23	~0.067	$\sim1.4\times10^{-10}$
95	Zr	65d	β	1.73	2.2	3.81	0.0408
99	Tc	2.1×10^5y	β	~0.13	0.156	~0.02	$\sim1.8\times10^{-10}$
103	Ru	40d	β	0.6	0.167	0.10	0.0017
106	Ru	1y	β	1.61	0.17	0.274	5.2×10^{-4}
107	Pd	7×10^6y	β	~0.02	0.072	~0.0014	$\sim4\times10^{-13}$
111	Ag	7.5d	β	~0.5	0.57	~0.28	~0.026
125	Sn	10d	β	~1.2	0.176	~0.21	~0.015
126	Sb	28d	β	~0.9	0.50	~0.45	~0.011
127	Sb	3.88d	β	~0.8	0.42	~0.34	~0.06
131	I	8.05d	β	0.50	1.73	0.865	0.0745
132	Te	3.21d	β	2.5	1.73	4.32	0.933
133	Xe	5.27d	β	~0.2	0.24	~0.048	~0.0063
135	Cs	2×10^6y	β	~0.1	0.244	~0.024	$\sim2.3\times10^{-11}$
137	Cs	30y	β	~0.55	0.45	~0.25	$\sim1.6\times10^{-5}$
140	Ba	12.8d	β	~2.4	0.45	~1.08	~0.058
141	Ce	32d	β	~0.27	0.45	~0.12	~0.0026
143	Pr	13.8d	β	~0.42	0.45	~0.189	~0.0095
144	Ce	285d	β	~1.5	0.45	~0.68	~0.0016
147	Nd	11.6d	β	0.45	0.09	0.040	0.0024
151	Sm	80y	β	~0.045	0.09	~0.004	$\sim1\times10^{-7}$
155	Eu	1.7y	β	~0.12	0.1	~0.012	$\sim1.3\times10^{-5}$
156	Eu	15d	β	~1.2	0.14	~0.17	~0.0078
161	Tb	7d	β	~0.3	0.15	~0.045	~0.0045
166	Dy	3.42d	β	~1	0.11	~0.11	~0.0223
169	Er	9.4d	β	~0.15	0.1	~0.015	~0.0011
171	Tm	1.9y	β	~0.05	0.05	~0.002	$\sim2\times10^{-6}$
175	Yb	4.2d	β	~0.23	0.03	~0.007	~0.0011
177	Lu	6.8d	β	~0.2	0.03	~0.006	$\sim6.1\times10^{-4}$
181	Hf	46d	β	~0.5	0.03	~0.015	$\sim2.3\times10^{-4}$
182	Ta	112d	β	0.8	0.057	0.046	2.85×10^{-4}
183	Ta	5.2d	β	~0.6	0.03	~0.018	~0.0024
185	W	74d	β	0.19	0.031	0.006	6.0×10^{-5}
188	W	65d	β	1.0	0.09	0.09	9.6×10^{-4}
189	Re	~200d	β	0.1	0.09	0.009	$\sim3.1\times10^{-5}$
191	Os	16d	β	~0.15	0.18	~0.027	~0.0012
194	Os	~2y	β	1.01	0.88	0.889	$\sim8.4\times10^{-4}$
196	Ir	9.7d	β	~0.6	0.278	~0.17	~0.012
199	Au	3.15d	β	~0.23	0.056	~0.013	~0.0028
203	Hg	48d	β	~0.23	0.056	~0.013	$\sim1.9\times10^{-4}$
210	Pb	20y	$\alpha+\beta$	5.8	0.17	0.986	9.36×10^{-5}
222	Em	3.8d	$\alpha+\beta$	23.1	0.034	0.785	0.143
223	Ra	11.6d	$\alpha+\beta$	28.6	0.034	0.972	0.058
224	Ra	3.6d	$\alpha+\beta$	28.7	0.045	1.29	0.248
225	Ra	14.8d	$\alpha+\beta$	27.9	0.045	1.26	0.059
226	Ra	1620y	$\alpha+\beta$	31.6	0.045	1.42	1.66×10^{-6}
227	Ac	22y	$\alpha+\beta$	34.8	0.032	1.11	9.57×10^{-5}
228	Ra	6.7y	$\alpha+\beta$	35.2	0.032	1.13	3.2×10^{-4}
229	Th	7300y	$\alpha+\beta$	33.8	0.032	1.08	2.8×10^{-5}
230	Th	8×10^4y	$\alpha+\beta$	36.4	0.123	4.48	1.06×10^{-7}
231	Pa	3.4×10^4y	$\alpha+\beta$	39.9	0.127	5.07	2.83×10^{-7}
232	Th	$1.39\times10^{10}y$	$\alpha+\beta$	39.3	0.641	25.2	3.43×10^{-12}

TABLE VIII,1.—*Continued.*

A	Element	Longest half-life, seconds, days or years	Decay type	Decay energy Q Mev	Initial abund. n_0 (Si $=10^6$)	Total energy n_0Q Mev	Initial en. rate $0.7\ n_0Q/t_{\frac{1}{2}}$ Mev/day
233	U	1.62×10^5y	$\alpha+\beta$	38.9	0.084	3.27	3.83×10^{-8}
234	U	2.50×10^5y	$\alpha+\beta$	41.2	0.084	3.46	2.63×10^{-8}
235	U	7.1×10^8y	$\alpha+\beta$	44.6	0.663	29.6	7.93×10^{-11}
236	U	2.39×10^7y	α	4.6	0.167	0.768	6.10×10^{-11}
237	Np	2.2×10^6y	$\alpha+\beta$	43.9	0.617	27.1	2.34×10^{-8}
238	U	4.51×10^9y	$\alpha+\beta$	46.3	0.405	18.8	7.90×10^{-12}
239	Pu	2.43×10^4y	α	5.2	0.267	1.39	1.08×10^{-7}
240	Pu	6.6×10^3y	α	5.3	0.110	0.583	1.68×10^{-7}
241	Am	$470y$	α	5.6	0.221	1.24	5.01×10^{-6}
242	Pu	3.8×10^5y	α	5.0	0.260	1.30	6.49×10^{-9}
243	Am	$7600y$	$\alpha+\beta$	5.4	0.157	0.848	2.0×10^{-7}
244	Pu	7.5×10^7y	$\alpha+\beta$	15.2	0.393	5.97	1.41×10^{-10}
245	Cm	1.1×10^4y	$\alpha+\beta$	11.4	0.430	4.90	8.43×10^{-7}
246	Cm	$4000y$	α	5.5	0.103	0.566	2.69×10^{-7}
247	Cm	$>4\times10^7y$	$\alpha+\beta$	16.3	0.103	1.68	$<7.76\times10^{-10}$
248	Cm	4.3×10^5y	α, SF(10%)	23.4	0.236	5.52	2.62×10^{-8}
249	Cf	$470y$	α	6.3	0.139	0.876	3.45×10^{-6}
250	Cm	7.5×10^3y	α, SF(75%)	170	0.139	23.6	5.97×10^{-6}
251	Cf	$700y$	α	6.2	0.236	1.46	3.96×10^{-6}
252	Cf	$2.2y$	α, SF(3%)	12.9	0.097	1.25	0.0011
253	E	$20d$	$\alpha+\beta$	6.7	0.188	1.26	0.0436
254	Cf	61 or $56.2d$	SF	220	0.139	30.6	0.349
255	E	$24d$	$\alpha+\beta$	7.3	0.139	1.01	0.0292
256	All	$\sim10^4s$	SF	...	...	...	...
257	Fm	$\sim10d$	α, SF(6%)	18.5	0.091	1.68	~0.116
258	All	$\sim10s$	SF, (n,f)	...	...	...	...
259	All	$\sim10s$	SF, (n,f)	...	...	...	...
260	All	$\sim10^{-2}s$	SF, (n,f)	...	...	...	...

odd A nuclei were produced, and that equal amounts of even A nuclei were produced, and that the ratio of production of odd to even A was 1:3. We feel that this assumption can be improved upon by using the results of Table VII,2. Table VII,2 includes the abundances which we have calculated for the r process in the range $A=71$ to 209. Estimates to be discussed later have been made for $A\leq70$. Above $A=209$ we include our calculations for the production of transbismuth mass numbers using exactly the same methods as those which were employed to calculate the abundance histogram shown in Fig. VII,3. The extended results are shown graphically in Fig. VII,4.

Some comments on the calculations above $A=209$ are appropriate. No guiding landmarks such as the observed magic number peaks are available above $A=209$. On the other hand, the relative masses of the nuclei near the beta-stable region are quite well established through extensive measurements of the alpha- and beta-decay energies of the naturally occurring and artificially produced radioactive nuclei from $A=210$ to ~260. This is amply demonstrated by the smoothness of the neutron binding energy excess curve shown in Fig. VII,1 for neutron numbers above $N=126$. The general increase in the neutron binding energy following the closure of the $N=126$ shell is apparent, as well as the rapid and considerable enhancement of stability which is to be attributed to the ability of the nucleons in nuclei with $N>126$ to take up spheroidal as contrasted to spherical distributions. The loss in neutron stability, after the maximum spheroidal deformation is reached at $N\sim140$ to 150, leads to a pseudo-shell effect‖ near $N=152$ for which there is considerable experimental evidence (Fig. VIII,1) in the sudden onset of spontaneous fission itself at this neutron number. The decrease in neutron binding energy leads to increased nuclear masses, and the energy available for fission suddenly increases. This increase, coupled with the already deformed shape which is the first step toward fission, leads to the catastrophic decline in spontaneous fission lifetimes.

Referring to Fig. VIII,3, the calculated and observed abundance curves just above the $N=126$ shell peak at $A=194$ show the precipitous drop expected from the rapid return to stability arising from the fact that the first neutrons in the $N=126-184$ shell deform these nuclei spheroidally. The greater neutron binding energy in the beta-stable region means that neutrons are readily captured, and that the capture path at $Q_n\sim2$ Mev passes through nuclei far removed from the stability line, the beta-decay energy at waiting points is enhanced, and the lifetimes and the resulting abundances are decreased ($A=200$ to $A=230$). Eventually, however, the maximum deformation is passed, and at $N=152$ the neutron binding energy is decreasing rapidly

‖ The next magic number expected after 126 on the shell model with strong spin-orbit splitting is $N=\frac{1}{3}[(n+1)^3+5(n+1)]=184$ for the $n=7$ shell.

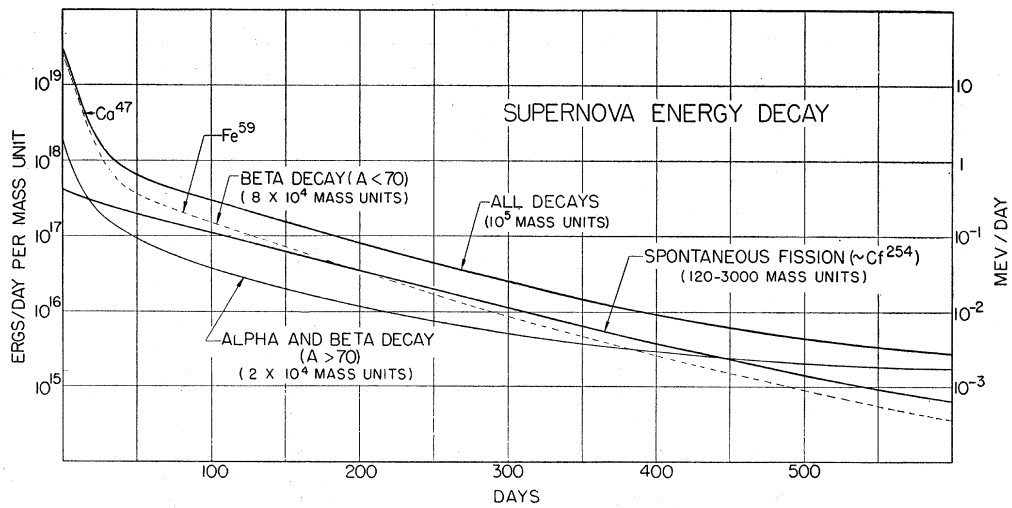

FIG. VIII,2. The radioactive energy release of the products of the r process. Radioactivity with half-lives less than 3 days has been neglected. Individual curves are shown for the beta decays of products with $A<70$, for alpha and beta decay for the products with $A>70$, for the products which decay by spontaneous fission, for the sum of all of these cases, and for Fe^{59} alone. The label for each curve includes the total mass in atomic mass units which produces the energy release measured in Mev/day on the right-hand ordinate. The scale of energy release in ergs/day, given in the left-hand ordinate, is for an amount of material measured in grams and equal numerically to the number of mass units indicated.

(Fig. VII,1), the r-process path moves toward the stability line, the beta decay waiting energy decreases, and the broad hump in the abundance curve from $A=230$ to ~ 260 corresponding to $N=152$ to 170 occurs. Included in this abundance hump is the progenitor of Cf^{254} at $A=254$. Superimposed on this broad hump is the minor peak expected at the closure of the $Z=82$ shell. Our calculations do not take into account the influence of the closing of the proton shell at $Z=82$ upon the neutron spatial distribution, which may tend to become more spherical at this point. This effect may well enhance, for the neutron-rich nuclei, the pseudo-shell effects at $N=152$, since some nuclei which lie in the r-process path fall close to having $N=152$ and $Z=82$ simultaneously.

Above $N=170$, $A=260$ the closing of the shell as N advances toward 184 would be expected to yield a deep minimum in the abundance curve just before a rise to another major peak at $N=184$, $A\sim 280$. However, the r process terminates before this minimum and subsequent rise can occur. This is because of the onset of neutron-induced fission (n,f) near $A\sim 260$, which will become more probable than neutron capture (n,γ) and will shunt the r-process products back to the middle of the periodic table at $A\sim 110$ and ~ 150, if we assume that asymmetric fission is the rule. These fission fragments are swept up in the general flow of the r process and in this way a cycling, steady flow will be established.

The sudden onset of neutron-induced fission is to be expected for exactly the same reasons as those previously enunciated to explain the onset of spontaneous fission. Even if neutron-induced fission were ignored, the 10^{-3} sec spontaneous fission lifetime will destroy the $A=260$ progenitors in an explosion for which the time-scale is 10–100 seconds. Even the mass chains at $A=257$, 258, 259 may not be produced in full measure. The onset of neutron-induced fission is delayed until $A\simeq 260$ only because the r process builds through neutron-rich nuclei for which the fission-inducing parameter Z^2/A is abnormally low, and also because the average neutron energy is moderately low ($kT\sim 100$ kev at $T\sim 10^9$ degrees). These last points constitute the central explanations underlying the difference between the fission decay curve of the californium fraction of the Bikini thermonuclear debris and the energy input curve expected for a Type I supernova. In the Bikini debris the 2.2-year Cf^{252} activity dominated the fission decay curve after about 200 days (Fi56) and indicated that 50 times as much Cf^{252} was produced as Cf^{254}. This factor of 50 is required because Cf^{252} decays only 3% of the time by spontaneous fission. In the thermonuclear test the capture path started with U^{238} and was limited to the neutron-rich isotopes of uranium ($Z=92$) even as it built through the progenitors of the beta-stable californium isotopes at 252 and 254. For the r process we see from Table VII,2 and Fig. V,2 that $Z=87$ and 88 at $A=252$ and $A=254$, respectively. Thus, the progenitors in the Bikini explosion had relatively higher Z and were more susceptible to neutron-induced fission as compared to neutron capture than are the progenitors in an r-process event. In addition, they were almost certainly subject to a neutron flux containing a high-energy component in the many Mev range and for this reason interacted relatively more often through fission than through capture. The result was certainly that the Bikini synthesis of the neutron-rich uranium isotopes (which ultimately decay to Cf^{252}, Cf^{254}, etc.) occurred only through an infrequent (1–10%) capture

event relative to fission at each mass number in the build-up from $A=238$ to 254. This competition with fission explains in a very plausible manner why, even though the high-energy neutron-capture cross section remained constant at the geometrical size of the neutron-rich isotopes of uranium, yet the relative synthesis must have decreased markedly with increasing A so as to have produced Cf^{254} only in the observed 2% of the amount of Cf^{252}. Thus, in the fission decay curve of the Bikini californium fraction, the Cf^{252} decay with its 2.2-year half-life should dominate, as it does, after about 200 days. This will not at all be the case in the r process where, as shown in Table VII,2, Cf^{252} and Cf^{254} are produced in the ratio of 0.097 to 0.139, essentially one to one.

We now return to the quantitative calculation of the radioactive energy decay curve which follows an r-process event. In Fig. VIII,2 is shown the energy release in ergs/day as a function of time for (i) the beta decays of nuclei with $A<70$, (ii) the alpha and beta decays with $A>70$, (iii) the spontaneous fission decay, and (iv) the total sum for these three cases. This figure is based on the calculations given in Table VIII,1, and these in turn are based on the abundance distribution for steady-state flow but without cycling from $A=110$ to 260. Figure VIII,2 thus represents the radioactive energy decay curve for an r-process event, such as might take place in a supernova outburst, which would have produced the atomic abundance distribution of Figs. VII,3 and VII,4 plus an extension to atomic weights below $A=70$. The main contributions to the energy release after the first few days through the first two years come from Ca^{47}, Fe^{59}, Ra^{228}, Cf^{252}, and Cf^{254}. These contributions are summarized in Table VIII,2.

Figure VIII,2 shows that the total energy release parallels the spontaneous fission release from 50 to 450 days. The spontaneous fission release during this period is almost entirely due to Cf^{254}. In the labels for each curve in Fig. VIII,2 we also include the total mass, in atomic mass units, involved in the production of each of the three types of decay given as (i), (ii), and (iii) above. Thus, the alpha- and beta-decay energy for $A>70$ in Mev/day (right-hand ordinate) is that for 2×10^4 atomic mass units of material which has been computed by multiplying the abundances of Table VII,2 by the appropriate atomic weights, A, and summing over $A>70$. In the left-hand ordinate we have obtained the energy release in ergs/day for the same numerical amount of material in grams by multiplying by 1.6×10^{-6} erg/Mev and dividing by 1.66×10^{-24} gram/atomic mass unit. The number of mass units producing the beta decay for $A<70$ is estimated to be 8×10^4 by extending the calculations of Table VII,3 in an approximate manner to $A<70$. Two estimates are given for the amount of mass associated with the spontaneous fission curve. If only the Cm^{250}, Cf^{254}, and Fm^{257} which actually undergo fission are counted, the total mass is some 120 atomic mass units. However, it is not possible to suppose that these fissionable products are produced alone and thus for another estimate we associate with them the production of all of the mass chains above $A=110$. This is the appropriate model for the situation discussed previously in which the neutron flux is great enough to move all of the material into the region $A=110$ to 260 and cycle it there. The yield from $A=110$ to 150 must be multiplied by one-half because only half of the fission fragments return to this region.

These considerations show that the energy release per gram of r product is much greater for fission than for alpha and beta decay. This is illustrated graphically in Fig. VIII,3 where the energy release is plotted for three different cases in which the same amount of material, namely, 1% of a solar mass (2×10^{31} g), is converted to r products. In Fig. VIII,3 the ordinate has been expressed in absolute magnitude with zero magnitude corresponding to 2.3×10^{40} ergs/day; this is done to facilitate comparison with actual supernova light curves which are shown and discussed in Sec. XII. A total

TABLE VIII,2. Principal radioactive decays of Table VIII,1.

A	Element	Longest half-life, days or years	Decay type	Decay energy Q Mev	Initial abund. n_0 (Si $=10^6$)	Total energy n_0Q Mev	Initial en. rate $0.7\ n_0Q/t_{\frac{1}{2}}$ Mev/day
33	P	25d	β	0.12	50	5.95	0.165
47	Ca	4.7d	β	1.83	100	183	26.9
59	Fe	45d	β	1.36	30	40.8	0.628
85	Kr	10.4y	β	0.31	3.4	1.05	1.9×10^{-4}
89	Sr	54d	β	0.66	3.4	2.24	0.0287
91	Y	58d	β	0.70	2.2	1.54	0.0183
95	Zr	65d	β	1.73	2.2	3.81	0.0408
131	I	8.05d	β	0.50	1.73	0.865	0.0745
140	Ba	12.8d	β	~2.4	0.45	~1.08	~0.058
144	Ce	285d	β	~1.5	0.45	~0.68	~0.0016
194	Os	~2y	β	1.01	0.88	0.889	$\sim8.4\times10^{-4}$
225	Ra	14.8d	$\alpha+\beta$	27.9	0.045	1.26	0.059
228	Ra	6.7y	$\alpha+\beta$	35.2	0.032	1.13	3.2×10^{-4}
250	Cm	7.5×10^3y	α, SF(75%)	170	0.139	23.6	5.97×10^{-6}
252	Cf	2.2y	α, SF(3%)	12.9	0.097	1.25	0.0011
254	Cf	61 or 56.2d	SF	220	0.139	30.6	0.349
257	Fm	~10d	α, SF(6%)	18.5	0.091	1.68	~0.116

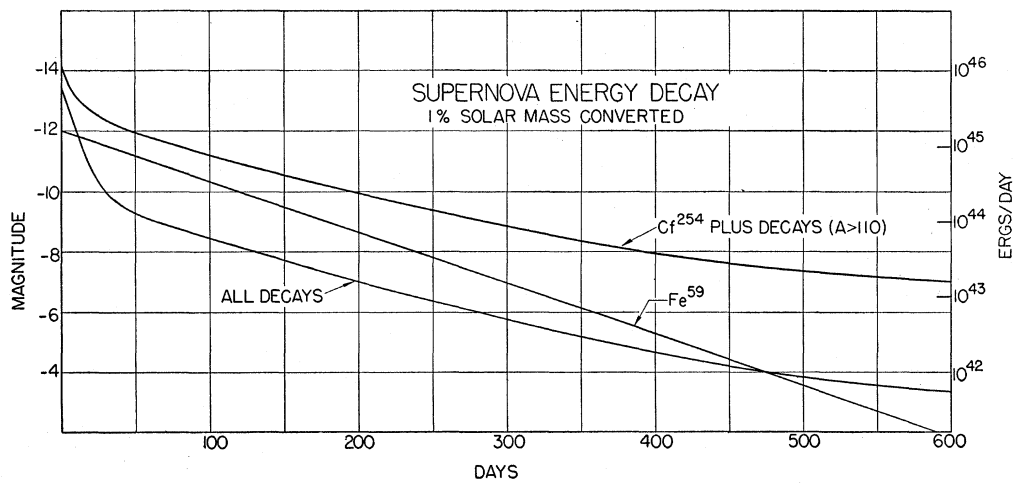

FIG. VIII,3. The radioactive energy release of the products of the r process calculated by assuming that one percent of a solar mass (2×10^{31} g) of these products is produced. Three cases are illustrated; (i) the energy release for all alpha, beta, and fission decays in relative abundances similar to those found for r-process products in the atomic abundance curve, (ii) the energy release for an extreme r-process event in which all of the converted material is moved into the region above $A=110$ and cycled there, and (iii) the energy release from Fe^{59}, when this isotope is produced in maximum quantity in a process in which only a few neutrons are made available per iron group nucleus. Compare with Fig. XII,1.

mass of one percent of a solar mass is taken simply as a reference point in this diagram. The total mass necessary to be converted to produce the observed light curves of supernovae is discussed for two specific cases, the Crab Nebula and the supernova in IC 4182, in Sec. XII.

The three cases which have been treated in Fig. VIII,3 are as follows. One case is the energy release for all activities in equilibrium with half-lives greater than 3 days, produced in an r process which would give an abundance distribution similar to that necessary to account for the r-process isotopes in the atomic abundance curve. This would occur, as indicated previously, if steady flow was achieved but no cycling occurred in the region above $A=110$. Another case illustrated is the energy release just for the activities produced above $A=110$. This is then the type of energy curve expected for a supernova in which the neutron flux was so great that all of the converted material was pushed into the region above $A=110$ and cycled there (one half cycling $A=110$ to 150). In this curve the Cf^{254} fission decay dominates the curve from 56 to 450 days but other activities take over after 450 days. The relation between this energy decay curve and the light curve of the supernova in IC 4182, which was observed for about 600 days after maximum, is also considered in Sec. XII.

The third case shown in Fig. VIII,3 is one calculated for the special case in which only a few neutrons are made available per iron group nucleus. In this case the most important activity produced is that of Fe^{59}, which has a half-life of 45 days. It is produced in maximum abundance when $n_c/Fe^{56}=3$, in which case 20% of the Fe^{56} is converted into Fe^{59} (Fo55a, Appendix II) and the remainder into nearby nuclei. The conditions under which the decay curve produced by Fe^{59} could explain an observed supernova light curve are discussed in Sec. XII, although from the astrophysical standpoint we do not consider this to be a very likely occurrence.

(2) *Abundance Yield in the r Process below $A=70$; the Production of Titanium; Discussion of Short-Period Radioactivity Following the r Process*

We have postponed to this point discussion of our estimate for the r-process yields below $A=70$. Two important activities, 4.8-day Ca^{47} and 45-day Fe^{59}, occur in this region. We have mentioned Fe^{59} above in discussion of a rather special possibility. Here we discuss its production in a steady-state r process similar to that discussed in Sec. VII when the abundances above $A=70$ were calculated. There is one important difference, however. When Fe^{56} is taken as the starting point (infinite source) in the r process, the first waiting point is at $A=68$, and no production below this atomic weight is achieved. Thus, the source material for building isotopes below $A\sim70$ must be the light elements rather than the iron group elements. This leads to considerable uncertainty in estimating the r-process yields below $A=70$.

Another reason why detailed calculations have not been made on the r process below $A=70$ is the fact that the s, e, and α processes are the major contributors in this region. Only for S^{36}, Ca^{46}, and Ca^{48} in this region is there no other method of production than the r process. It is also possible that Ti^{47}, Ti^{49}, and Ti^{50} should be assigned to this process. All of these isotopes except Ca^{46} have abundances ~100 (Su56). Thus empirical data in this region are lacking. Although good mass data are

available, we have hesitated to use our expression for the effective W_β for light nuclei in calculating τ_β and hence abundances, since it assumes a high density of levels in the daughter product. Since the abundance is proportional to W_β^{-5}, one can expect considerable fluctuations for the r-process products. This may explain the behavior illustrated by the abundance ratios $Ca^{46}:Ti^{47}:Ca^{48}=1.6:189:88$. An abundance peak for $N=28$ in the r process might be expected at somewhat lower A, and thus the abundance of Ca^{46} seems definitely low and must be attributed to a fluctuation in the value of W_β at the progenitor for $A=46$. Ti^{47} may also be produced in the s process or possibly in the e process. The abundance produced in the s process should be considerably less than the abundances of Sc^{45} and Ti^{46}, which are 63 and 194, respectively, since the s process is dropping rapidly in this region. It should also be produced less abundantly than $Ti^{46}(194)$, $Ti^{49}(134)$, and $Ti^{50}(130)$ in the e process. Thus it would seem reasonable to attribute to the r process a part of the mass-chain at $A=47$ comparable in abundance to Ca^{48} rather than to the abnormally low Ca^{46}. Ca^{47} is in this chain and we round off its abundance to about 100 as given in Table VIII,1. As indicated in Fig. VIII,2, this gives rather a large contribution in the early part of the energy decay curve. However, as discussed in Sec. XII, the early part of the supernova light curve may not be simply a radioactive energy decay curve, since it may represent cooling of the expanding envelope for a short period after the explosion.

The amount of production of the mass-chain at $A=59$, and of Fe^{59} in particular, is very difficult to estimate. We can expect that the nucleus produced directly in the r process might have $Z=20$. An atomic abundance estimate of 30 is a reasonable value. The energy release in the decay of the Fe^{59} is slightly larger than that in the decay of the Cf^{254} when the atomic abundance yield of the Fe^{59} is assumed to be 30. The abundances are in the ratio $30/0.139\simeq 220$ while the energy release ratio is $1.35/220=1/160$. The Ca^{47} energy release is ~ 5 times that of Cf^{254}. This, of course, will not be the case in a supernova in which a large ratio of neutrons to iron is available and only activities with $A>110$ are produced. However, this illustrates the fact that in any case the energy release in the Cf^{254} is only a small part of the *total* energy release from the radioactivity following a supernova explosion. In each mass-chain there will be very rapid beta decays releasing some 10 Mev in beta-ray energy. We estimate that the Cf^{254} is only about 0.05 to 0.5% by number of all the nuclei produced in the r process. Thus the total energy released radioactively is 10 to 100 times that from Cf^{254} but is emitted within a matter of a few minutes or hours of the initial explosion. The main point is this: If the Cf^{254} release is $\sim 10^{47}$ ergs, which is a reasonable estimate, then the total radioactive energy release will be 10^{48} to 10^{49} ergs. This is indeed a large value, but it does not exceed the total energy available, some 10^{50} ergs, from the hydrogen and helium reactions which take place in the envelope of the supernova.

(3) *Abundance of Fission Fragments Produced in the r Process*

At this point a remark concerning the contribution of fission fragments to the atomic abundance distribution is in order. Termination of the r process by very rapid spontaneous fission and neutron-induced fission during the supernova explosion will occur at $A\sim 260$, $Z\sim 90$. Fission of such neutron-rich nuclei will probably result in the production of more neutrons than are observed for beta-stable nuclei; we estimate ~ 6. On the assumption that the fission is asymmetrical in charge and mass we then expect fragments which are spread about $A\sim 108$, $Z\sim 38$, and $A\sim 146$, $Z\sim 52$, as shown diagrammatically in Fig. V,2, although we have rounded off these numbers to $A=110$ and 150 in preceding discussions. The neutron-rich fragments are very similar to the nuclei involved in the capture path and are swept up into the r process and do not produce any particular effects near $A\sim 108$ or 146. They tend to cycle material above $A\sim 108$ and to establish steady-state abundances in this region, even though they are far from the iron group elements and light elements with which the synthesis starts. The neutrons released in the fission are recaptured as the r process proceeds.

On the other hand, the ultimate decay by spontaneous fission of Cm^{250}, Cf^{252}, Cf^{254}, and Fm^{257} produces a total yield of both light and heavy fragments equal to $0.75\times 0.139+0.03\times 0.097+0.139+0.06\times 0.091=0.252$ on the $Si=10^6$ scale (see Tables VII,2 and VIII,1). This abundance is spread out over the usual distribution in fragments and the peak yield can be expected to be about 8% of the total or about 0.020. This is illustrated graphically in Fig. VII,3, where it will be noted that the fission fragment abundance is small compared to that produced directly in the r process.

C. Age of the Elements and of the Galaxy

Transuranium elements are produced by the r process. Those with atomic weights of the form $235+4m$, $m=0, 1, 2, 3\cdots$ are progenitors of U^{235} provided alpha decay is more probable than fission. From Table VIII,1 this appears to be the case for $m\leq 5$ but for $m>5$ it seems that fission must dominate. Thus there are six progenitors of U^{235} at atomic weights 235, 239, 243, 247, 251, and 255. The number of progenitors of U^{238}, of atomic weights $238+4m$, is even more restricted. As can be seen in Table VIII,1 the beta-stable nuclei at $A=238$, 242, and 246 decay by alpha emission while that at $A=250$ decays 25% of the time by alpha emission and 75% by fission. Starting with Cf^{254}, nuclei of atomic weights 254, 258, etc., decay predominantly by fission. This information is summarized in Table VIII,3, where we also list the progenitors of the other parents of the radioactive series, Th^{232} and Np^{237}.

TABLE VIII,3. Production of parents of radioactive series; progenitors decaying by alpha emission rather than spontaneous fission.

Half-life	$_{90}Th^{232}(4n)$ $1.39\times10^{10}y$		$_{93}Np^{237}(4n+1)$ $2.2\times10^{6}y$		$_{92}U^{238}(4n+2)$ $4.51\times10^{9}y$		$_{92}U^{235}(4n+3)$ $7.13\times10^{8}y$	
	A	Yield	A	Yield	A	Yield	A	Yield
	232	0.084	237	0.057	238	0.110	235	0.057
	236	0.057	241	0.221	242	0.157	239	0.110
	240	0.110	245	0.103	246	0.103	243	0.157
	244	0.157	249	0.139	250(25%)	0.035	247	0.103
	248	0.139	253	0.097			251	0.097
	252(97%)	0.094					255	0.139
Total yield		0.641		0.617		0.405		0.663

Ratio $U^{235}/U^{238}=0.663/0.405=1.64$
$Th^{232}/U^{238}=0.641/0.405=1.58$

If the abundances produced by the r process were the same for all progenitors, the ultimate abundance of U^{235}, after alpha and beta decays at 239, 243, etc., would exceed that of U^{238} by a factor of $6/3.25=1.85$. Calculations discussed in the previous sections make it possible to improve upon this factor by totaling the yield of the progenitors for the individual radioactive parents, U^{235}, U^{238}, and Th^{232}, Np^{237} as well. Yields for the progenitors and the totals after alpha and beta decay are given in Table VIII,3. The ratio of U^{235}/U^{238} produced by the r process and subsequent decay is 1.64, slightly less than the ratio of the number of progenitors. This is to be expected since the even-A progenitors of U^{238} will individually be produced in greater abundance than the odd-A progenitors of U^{235} because of the even-odd pairing term which decreases the beta-decay energy of even-A waiting points and thus increases even-A waiting point abundances. This effect is most clearly demonstrated by the calculations in Sec. VII which show peaks at $A=130$ and 194, where each A is a waiting point. We digress, in order to discuss this effect more fully.

For the $A=130$ peak, results of the calculations given in Table VII,2 are that $W_\beta=11.46$, 9.30, and 9.61 Mev at $A=125$, 126, and 127, respectively. For $A=126$ the value would have been $W_\beta=10.50$, i.e., it would have been intermediate between the values for 125 and 127, if we had not subtracted $\delta_A/2=1.20$ Mev from this value. The calculated abundances were then found to be 0.18, 0.50, and 0.42, and these values must be compared with the observed values for Te^{125}, Te^{126}, and I^{127}, i.e., 0.328, 0.874, and 0.80. The computed values are low but are relatively correct. Empirically, we can estimate the even-odd pairing effect from $2Te^{126}/(Te^{125}+I^{127})=1.55$. The main uncertainty in this calculation arises from the uncertainty in the abundance ratio of tellurium to iodine.

Three osmium isotopes are produced in the rising portion of the $A=194$ peak. Using $\delta_A/2=0.78$ Mev, we find that $W_\beta=13.06$, 13.14, and 11.54 Mev at $A=188$, 189, and 190, respectively. The predicted abundances are then 0.09, 0.09, and 0.17, and these are in good agreement with the observed abundances of Os^{188}, Os^{189}, and Os^{190}, which are 0.133, 0.161, and 0.264, respectively. In this case, on the basis of relative isotopic abundances alone, the even-odd pairing term is given by $(Os^{190}+Os^{188})/(2\times Os^{189})=1.23$. Incidentally, the observed abundance ratio of the two osmium isotopes $Os^{190}/Os^{188}=1.98$ represents a substantial check on our calculated abundances (proportional to W_β^{-5}), which give a ratio of 1.85. This agreement indicates that our choice of parameters B_A and Z_A and our use of $W_\beta=B_A(Z_A-Z-2.5)+$pairing term has some empirical validity. Off the abundance peaks, the even-odd effects are not so clear cut in our method of calculation, since odd-A nuclei can result from even-A waiting points and vice versa. However, there is some correlation along even and odd lines as is clear from a perusal of Table VII,2.

An even-odd effect of 1.13 yields the change from 1.85 to 1.64 discussed above for the uranium isotopes, and this seems to be a reasonable value. It neglects the effect of delayed neutron emission from excited states of the nuclei in the decay of the various mass chains to their stable isobars. This is a small effect, but does give some transfer of even-A material to odd-A material since the most highly excited states result in beta transitions from odd Z-odd N-even A nuclei to even Z-even N-even A nuclei. If the even-odd effect were as high as 1.55, as it is at the $A=130$ peak, the production ratio would be 1.20. By a selective choice of parameters entering into our calculation the ratio could be reduced in extremum to a value as low as unity. It is our considered opinion that it is highly unlikely for the ratio to be less than this value. A reasonable value for an upper limit would be 2.

With these estimates of the production ratio of U^{235}/U^{238} in the r process, we are now able to calculate the age of these uranium isotopes (and by inference of the other r-process isotopes) using their presently observed terrestrial abundance ratio.

(i) Let us suppose that all of the uranium were produced in a single r-process event (e.g., one supernova) at one moment of time, $t_0\times10^9$ years ago. Then, using a present-day ratio of $U^{235}/U^{238}=0.0072$, and using half-lives of 7.13×10^8 years and 4.51×10^9 years for U^{235} and U^{238}, respectively, we have the following equa-

tion for the abundance ratio U^{235}/U^{238} as a function of t_0

$$\frac{U^{235}(t_0)}{U^{238}(t_0)}=0.0072\times 2^{t_0[(1/0.713)-(1/4.51)]}=0.0072\times 2^{1.18t_0}.$$

This relationship is plotted in Fig. VIII,4. At the formation of the solar system 4.55×10^9 years ago $U^{235}/U^{238}=0.29$, which is definitely below the lower limit of unity for the production ratio discussed above. We find $U^{235}/U^{238}=1$, 1.64, and 2 at $t_0=6.0$, 6.6, and 6.9×10^9 years, respectively. Our best value for the time of a single-event synthesis of U^{235} and U^{238} is thus 6.6×10^9 years ago. If these isotopes were produced in a single supernova, this is its date. For each change of a factor of two in the production ratio of the uranium isotopes, this figure changes by 0.85×10^9 years.

There is some confirmatory evidence for the above calculations in the Th^{232}/U^{238} abundance ratio, which is, however, much more uncertain than the U^{235}/U^{238} ratio. Suess and Urey estimate that the present-day ratio $Th^{232}/U^{238}=3$ to 3.5. Our production ratio is $0.641/0.405=1.58$. From these data we find $t_0=6.2$ to 7.7×10^9 years. This time estimate is obviously quite sensitive to the value taken for the present thorium to uranium ratio but is not inconsistent with the value of t_0 obtained from the U^{235}/U^{238} ratio.

(ii) Alternatively, let us consider the problem on the basis that production of uranium started a time $t_0\times 10^9$ years ago and that, instead of production being confined to just one moment, production took place at a constant rate until a time $t_1\times 10^9$ years ago, after which no more production occurred. This model corresponds to production in a series of supernovae with uniform mixing of their products over the interval t_0 to t_1. Let $U^{235}(t)$ and $U^{238}(t)$ be the abundances at any time, t, and let λ_{235} and λ_{238} be the production rates taken as independent of time. If t is taken as the time measured backward from the present epoch, we then have

$$\left.\begin{aligned}-\frac{dU^{235}(t)}{dt}&=\lambda_{235}-\frac{0.693}{0.713}U^{235}(t)\\ -\frac{dU^{238}(t)}{dt}&=\lambda_{238}-\frac{0.693}{4.51}U^{238}(t)\end{aligned}\right\}\quad t_0\geq t\geq t_1.$$

These equations taken together with the boundary conditions

$$U^{235}(t_0)=U^{238}(t_0)=0$$

integrate to give

$$\frac{U^{235}(t)}{U^{238}(t)}=\frac{0.713\lambda_{235}[1-2^{-[(t_0-t)/0.713]}]}{4.51\lambda_{238}[1-2^{-[(t_0-t)/4.51]}]}\quad t_0\geq t\geq t_1.$$

This result, together with the condition that the free decay of U^{235} and U^{238} from t_1 to the present day must yield a ratio equal to 0.0072, determines the following

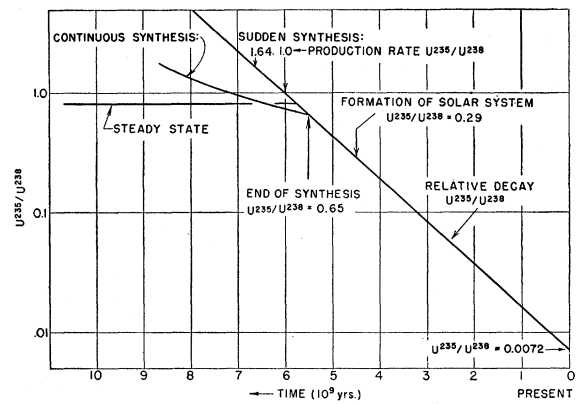

FIG. VIII,4. The ratio U^{235}/U^{238} as a function of time. This curve has been employed to determine the age of terrestrial uranium by the method described in Sec. VIII C.

relation between t_1 and t_0

$$\frac{U^{235}(0)}{U^{238}(0)}=\frac{0.713\lambda_{235}[1-2^{-[(t_0-t)/0.713]}]2^{-t_1/0.713}}{4.51\lambda_{238}[1-2^{-[(t_0-t)/4.51]}]2^{-t_1/4.51}}=0.0072.$$

With

$$\lambda_{235}/\lambda_{238}=1.64,$$

this reduces to

$$\frac{[1-2^{-[(t_0-t_1)/0.713]}]}{[1-2^{-[(t_0-t_1)/4.51]}]}\times 2^{-1.18t_1}=\frac{0.0072\times 4.51}{1.64\times 0.713}=0.0278.$$

The values of t_0 corresponding to a set of values of t_1 are given in the following tabulation, along with values of $U^{235}(t_1)/U^{238}(t_1)$:

t_1 (in 10^9 years)	4.5	5.0	5.5	6.0	6.6
t_0 (in 10^9 years)	18	11.5	8.5	7.4	6.6
$U^{235}(t_1)/U^{238}(t_1)$	0.29	0.43	0.65	0.98	1.64

The computed value for t_0 is very sensitive to t_1 if t_1 is chosen near the time of formation of the solar system at about 4.5×10^9 years ago. On the other hand, t_0 does not change rapidly once t_1 exceeds 5.5×10^9 years ago, since t_0 must equal t_1 at 6.6×10^9 years, the computed time for a single-event synthesis. Evidence on the time interval between nucleogenesis and the formation of the meteorites of the solar system has been given by Wasserburg and Hayden (Wa55b). Following Suess and Inghram they argue that Xe^{129} would be abnormally abundant in meteorites if the meteorites crystallized before I^{129}, with an observed half-life of 1.7×10^7 years, had all decayed. They did not find abnormal amounts of Xe^{129} in the Beardsley chondrite and concluded that it crystallized at least 23.7 half-lives or 4.1×10^8 years after the production of the I^{129}. In their argument they assume that I^{129} and I^{127} were produced in equal amounts. This is consistent with our point of view that I^{129} is a progenitor of Xe^{129} and Suess and Urey's abundance ratio $Xe^{129}/I^{127}=1.05/0.80=1.30$. Our calculations in Table VII,2 yield $I^{129}/I^{127}=1.17/0.42=2.8$ in

the r process. Actually, the calculations of Wasserburg and Hayden are quite insensitive to the I^{129}/I^{127} ratio, our calculated value raising their lower limit only to 4.3×10^8 years.

On this basis it would seem justified to choose $t_1\geq5.0\times10^9$ years, and therefore t_0 lies between 11.5 and 6.6×10^9 years. For nucleogenesis in a continuous and uniform series of supernovae occurring between the formation of the galaxy and the time of formation of the cloud of gas or protostar from which the sun condensed, we can take 10^{10} years as a round figure for the beginning epoch. On this point of view the age of our galaxy is thus $\sim10^{10}$ years.

There is one point of view in which the above ideas must be somewhat modified. In the steady-state cosmologies of Hoyle (Ho49) and of Bondi and Gold (Bo48) it may be expected that the U^{235}/U^{238} ratio in a sufficiently large volume will remain constant due to supernova activity, in spite of the apparent universal expansion and the constant dilution by the addition of matter in the form of hydrogen which is necessitated in order to keep the mass energy content of the specified volume at a fixed value. The characteristic time involved for the removal by expansion of one-half of a particular type of matter from a fixed volume is $0.693T/3$, where T is the reciprocal of Hubble's constant. Taking T as 5.4×10^9 years we have for our characteristic half-life 1.25×10^9 years. The decay lifetime for any radioactive material must be properly corrected for this value. The effective lifetimes of U^{235} and U^{238} become 0.45×10^9 and 0.98×10^9 years, respectively.

On the steady-state point of view $t_0=\infty$, and after a long period of production one would expect that at time t_1, after which no further contribution to solar system material occurred, we should have

$$\frac{U^{235}(t_1)}{U^{238}(t_1)}=\frac{0.45\lambda_{235}}{0.98\lambda_{238}}=0.75.$$

This is just the value expected from the present-day ratio of $U^{235}/U^{238}=0.0072$ now if the solar system material has been isolated for some 5.7×10^9 years. We may conclude that the present abundance ratio of the uranium isotopes is consistent with the steady-state cosmology if the method of production of their isotopes is the r process as described. We do not wish to overemphasize this conclusion, but rather to emphasize that studies concerning the origin of the radioactive elements may lead to objective tests of the various cosmological theories.

It can also be noted that there exists an approximate indication of the epoch of synthesis by the s process. The radioactive isotope K^{40} is in the main line of the s process. Figure VI,1 shows that for this isotope $\sigma N\sim10^4$ for σ in mb and N on the scale $Si=10^6$. We estimate in the appendix that $\sigma\sim100$ mb so at the time of K^{40} production $N\sim100$. It is now, $N=0.38$. Using the known K^{40} half-life of 1.3×10^9 years we find that the K^{40} was produced $\sim10^{10}$ years ago. This calculation could be made with great assurance if the capture cross sections for 15-kev neutrons were measured accurately for K^{39}, K^{40}, and K^{41}. Our calculation assumes the K^{40} cross section to be 12.5 times that of K^{39} which has a closed shell of neutrons.[20] Even if this factor has the very high value of 100 the epoch for K^{40} formation will be reduced only to 6.5×10^9 years ago.

In any case we consider the minimum age of the isotopes of uranium, namely 6.6×10^9 years with an uncertainty on the low side of at most 0.6×10^9 years, to be significantly greater than the age of the solar system, 4.5×10^9 years. This age is indeed comparable to the ages, 6.5×10^9 years, of the oldest known clusters in the galaxy (Jo56, Ho55, Ha56c). Since our age is a minimum for that of the elements and thus, on the hypothesis of stellar nucleogenesis, for the galaxy, it would not be unexpected if still older objects were eventually found in the galaxy.

D. Termination of the s Process; the Abundances of Lead, Bismuth, Thorium, and Uranium

The s process is terminated at Bi^{209} by the onset of natural alpha-particle radioactivity. Detailed discussion of the termination has been postponed to this point so that it can be applied, along with the discussion of the r-process termination, to calculation of the abundances of lead, bismuth, thorium, and uranium, which can be expected to be produced in the s and r processes.

As illustrated in Fig. VIII,5, the s process proceeds through the mercury isotopes to stable Tl^{203} and thence by neutron capture to Tl^{204} which decays 98% by beta emission to Pb^{204} and 2% by electron capture to Hg^{204}. We can neglect this last branching. The half-life of Tl^{204} is 4.1 years, which we shall take to be short compared to its mean neutron-capture time. At Pb^{204} neutron capture leads to Pb^{205} which decays by electron capture with a lifetime of approximately 5×10^7 years to Tl^{205}.

Pb^{205} is essentially stable on the time-scale of individual captures in the s process, and the neutron capture continues through the stable lead isotopes Pb^{206}, Pb^{207}, and Pb^{208} to beta-active Pb^{209}. After the s process finally ends, the Pb^{205} produced in the capture chain eventually does decay to Tl^{205}. Pb^{209} decays in 3.3 hours to stable Bi^{209} which, upon neutron capture, forms the 2.6×10^6-year alpha-particle-emitting ground state of Bi^{210} or the 5.0-day electron-emitting isomeric state, RaE. For slow neutrons the capture results 44% of the time in the ground state and 56% of the time in the isomeric state. It is reasonable to assume that this branching ratio will hold for the 15-kev neutrons involved in the s process. The RaE decays quickly before neutron capture to Po^{210} which is an alpha-particle emitter with 138.4-day half-life, fast compared to neutron capture times. Thus Pb^{206} is

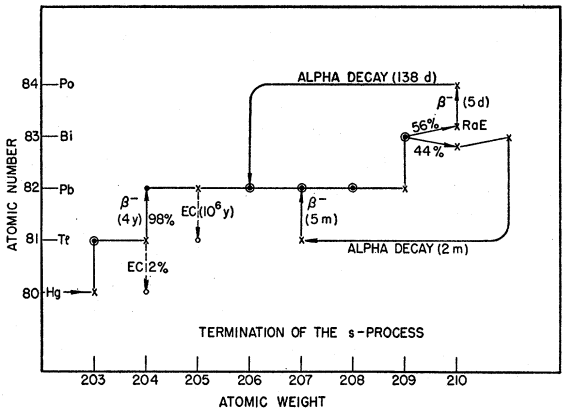

FIG. VIII,5. This diagram shows the details of the termination of the s process. The half-life for electron capture in Pb^{205} should be changed to $\sim 5\times 10^7$ years.

formed and this branch of the termination of the s process can result in a cycling process between Pb^{206} and Bi^{210}. The long half-life of the ground state of Bi^{210} means that it captures a neutron before decaying, so that in this case the termination is delayed until Bi^{211} is formed; this then decays rapidly through Tl^{207} to Pb^{207}, which can then cycle back through lead and bismuth. The result is a steady production of Pb^{206}, Pb^{207}, Pb^{208}, and Bi^{209} by the s process. The steady-flow relative abundances of these nuclei are then given by

$$an_{204}\sigma_{204}=an_{205}\sigma_{205}=1.8n_{206}\sigma_{206}$$
$$=n_{207}\sigma_{207}=n_{208}\sigma_{208}=n_{209}\sigma_{209},$$

where the σ's represent neutron capture cross sections, a is the factor for the number of terminal cycles, and the factor $1.8=1+44/56$ arises because Pb^{206} is replenished in only 56% of the cycling processes.

The capture cross section for 15-kev neutrons have been discussed in Sec. V and are given in the appendix. These cross sections are 100 and 50 mb for the odd isotopes Pb^{205} and Pb^{207}, 25 mb for the even isotope Pb^{206}, 10 mb for the even doubly-magic isotope Pb^{208}, and 15 mb for the odd magic Bi^{209}. These values are consistent with the energies gained on neutron addition, i.e., 8.10, 7.38, 6.73, 3.87, and 4.67 Mev, respectively. There is a problem concerning the neutron addition energy and the capture cross section for Pb^{204}. The reactivity measurements do not distinguish between even isotopes. From Huizenga's masses (Hu55) the energy is 6.80 Mev but has a considerably larger error than that for the other lead isotopes. It can be argued that Pb^{204}, with fewer neutrons than Pb^{206}, should more readily capture neutrons than Pb^{206}, and so the Pb^{204} cross section has been estimated as 50 mb. On this basis one-half as much Pb^{204} should be produced on the s process as Pb^{206}, as long as cycling is neglected. To see whether such a ratio is reasonable, we may compare it with the abundance ratios of other pairs of even isotopes which have been made in a similar way, i.e., by steady flow in the s process without cycling. We find, for example, that the abundance ratios $Te^{122}/Te^{124}=0.52$, $Xe^{128}/Xe^{130}=0.47$, $Ba^{134}/Ba^{136}=0.31$, and $Sm^{148}/Sm^{150}=1.52$.

An alternative way of estimating the relative lead capture cross sections is by comparison with the barium capture cross sections deduced from the relative abundances of the barium isotopes 134, 135, 136, 137, and 138. These lead to the completion of the $N=82$ neutron shell just as Pb^{204} to Pb^{208} lead to the completion of the $N=126$ shell. Ba^{134} and Ba^{136} are shielded, that is, they are made only in the s process, Ba^{138} is magic in the s process and all of its yield can be attributed to this process, while for Ba^{135} and Ba^{137} we have attributed two thirds of their abundances to the s process.

Thus, on the basis of our two independent estimates, the relative abundances of the lead isotopes produced in the s process are as follows:

	Pb^{204}	Pb^{205} (Tl^{205})	Pb^{206}	Pb^{207}	Pb^{208}	Bi^{209}
From reactivity σ	1	0.5	$1.1a$[a]	a	$5a$	$3.3a$
From barium abundances	1	1.8	$1.8a$[b]	$3.1a$	$29.6a$	···

[a] In case $a=1$, use 2 in place of $1.1a$.
[b] In case $a=1$, use 3.2 in place of $1.8a$.

Having discussed the relative abundances of the lead isotopes and bismuth expected to be produced by the s process, we must now calculate the relative abundance production expected in the r process. This can be done for Pb^{206}, for example, by first adding the abundances given in Table VII,2 for the mass chains 206, 210, 214, . . . 234, which decay fairly rapidly to Pb^{206}. For Pb^{206} this sum is 0.48 on our customary scale. If we wish to compare our results with the "nonradiogenic" lead isotope abundances at the time of formation of the solar system, we must add to this sum the amount of Pb^{206} resulting from the decay of U^{238} in the period between element production and solar system formation. This value depends somewhat on whether the element formation was continuous, or occurred in a single event, but for simplicity we have chosen the latter alternative. The decay period is then $(6.6\text{–}4.5)\times 10^9=2.1\times 10^9$ years, so that 27% of the U^{238} will have decayed. From Table VIII,3 we see that this adds 0.11 to the Pb^{206} abundance, bringing the total to 0.59. These abundances are summarized in Table VIII,4 which also includes the results of similar calculations for Pb^{207}, Pb^{208}, and Bi^{209}. Since Np^{237} decays rapidly as compared with the time scales involved here, the Bi^{209} abundance is just the sum over all mass chains 209, 213 . . . 253.

For the nonradiogenic lead isotope abundances it is customary to take the isotopic abundances observed in iron meteorites, which have the lowest observed proportions of radiogenic leads, and which are assumed to have crystallized without including parents of the radioactive series [see discussion on p. 68 of (Su56)]. For the present-day average for lead, Suess and Urey

recommend the chondritic meteorite ratios. According to Patterson *et al.* (Pa53, Pa55, Pa55a) the ratios are

	$\frac{Pb^{206}}{Pb^{204}}$	$\frac{Pb^{207}}{Pb^{204}}$	$\frac{Pb^{208}}{Pb^{204}}$	$\frac{\text{Total Pb}}{Pb^{204}}$
Iron meteorites, 4.5×10^9 yr ago	9.5	10.3	29.2	50.0
Chondrites "now"	19.4	15.9	38.6	74.9

Now Pb^{204} is not produced directly in the r process, since it is shielded by Hg^{204} and it does not result from any radioactive decay of r products. From the capture cross sections in the s process it may be expected that it will be produced to a lesser extent than the other isotopes, and this will be especially true if the s process does not just terminate at Bi^{209}, but cycles to some extent, thus building up Pb^{206}, Pb^{207}, and Pb^{208}. Thus the observed ratios given above are entirely reasonable on the basis of s process and r process synthesis of the elements.

On the other hand, these processes will have produced much more lead than commonly accepted in abundance estimates. This can be seen as follows. Pb^{204} is produced in the regular flow of the s process, and should have the corresponding abundance, which may be calculated as follows. The average value of σN, read off the curve in Fig. VI,3, is about 10 in the vicinity of $A=204$. The estimate given above for the cross section is 50 mb, and hence $N=0.20$. The cross-section estimate is probably high rather than low, so this abundance is, if anything, a lower limit. This leads to a total lead abundance of 10 for the iron meteorites and 15 for the chondrites. These values are much larger, for example, than those given by Suess and Urey, namely 0.31 and 0.47, respectively. On the other hand, our values are in good agreement with the solar abundance obtained by Goldberg *et al.* (Go57), i.e., a value of about 20 from the lead/hydrogen ratio and 10 from the lead/silicon ratio on the silicon$=10^6$ scale. Our view is that the meteoritic abundance of lead may be exceptionally low due to a fractionating process that took place when the meteorites were formed.

TABLE VIII,4. Production of Pb^{206}, Pb^{207}, Pb^{208}, and Bi^{209} in the r process.

	Pb^{206}	Pb^{207}	Pb^{208}	Bi^{209}
Long-lived parent	U^{238}	U^{235}	Th^{232}	(Np^{237})
Parent:				
Originally	0.405	0.663	0.641	0.617
4.5×10^9 years ago	0.295	0.083	0.577	0.0
Now	0.146	0.001	0.462	0.0
From long-lived parent:				
4.5×10^9 years ago	0.110	0.580	0.064	0.617
Now (no fractionation)	0.259	0.662	0.179	0.617
Short-lived progenitors	0.477	0.369	0.266	0.317
Total:				
4.5×10^9 years ago	0.587	0.949	0.330	0.934
Now (no fractionation)	0.736	1.031	0.445	0.934
Radiogenic	0.149	0.082	0.115	0.0

On the basis of our analysis of the lead produced in the s and r processes we can calculate lead isotope ratios, the only uncertainty being in the cycling factor a. Using the two estimates of the cross sections discussed above, i.e., those derived from the reactivity measurements and those derived from the barium abundances [with $\sigma(Pb^{204})=50$ mb], and choosing $a=6$ in the first case and $a=1$ in the second, we have the following values for the three isotopic ratios:

	$\frac{Pb^{206}}{Pb^{204}}$	$\frac{Pb^{207}}{Pb^{204}}$	$\frac{Pb^{208}}{Pb^{204}}$	$\frac{Bi^{209}}{Pb^{204}}$
From reactivity $\sigma(a=6)$	9.5	10.7	31.6	24.7
From barium abundances ($a=1$)	6.2	7.8	31.2	···
Iron meteorites (obs)	9.5	10.3	29.2	···

In this calculation we have taken into account the amount of lead produced by the decay of r-process isotopes before the freezing of the material of the meteorites 4.5×10^9 years ago. Thus for the first case ($a=6$), $Pb^{206}/Pb^{204}=1.1\times6+0.587/0.2=9.5$. There is little to choose between the two sets of calculations, but we are inclined to favor the first since it would be rather accidental if the s process terminated at bismuth without some cycling at its termination.

In addition to obtaining a high abundance of lead through these calculations, we also find that the abundance of bismuth is high. Using the reactivity cross sections and the cycling factor $a=6$, we find that Bi^{209} should be produced with an abundance 20 times that of Pb^{204} in the s process. An additional contribution of $0.934/0.2=4.7$ comes from the r process (Table VIII,4). Thus, Bi^{209} should have an abundance of $24.7\times0.2=4.94$ on the silicon$=10^6$ scale whereas Suess and Urey, using a value due to the Noddacks, give 0.144.

On the other hand, our calculation of the abundances of the isotopes of thallium is in fair agreement with the abundances given by Suess and Urey. Thus Tl^{203}, with a cross section of 276 mb, has a calculated s-process abundance of $10/276=0.036$, to which must be added 0.057 from the r process, yielding a total of 0.093 which is only a factor of 3 higher than the Suess and Urey value of 0.0319. Tl^{205} results from the decay of Pb^{205} produced in the s process and thus the Pb^{205} cross section of 100 mb must be used in calculating its s-process abundance, i.e., $10/100=0.10$. Adding 0.057 for the r-process abundance, we obtain 0.157 which is about twice the value of 0.0761 given by Suess and Urey.

Our values for the mercury isotopes, as compared with the values of Suess and Urey, are shown in the following:

	s process	r process	Total	Suess and Urey
Hg^{196}	0.0	0.0	(p process)→	0.00045
Hg^{198}	0.042	0.057	0.099	0.0285
Hg^{199}	0.015	0.057	0.072	0.0481
Hg^{200}	0.042	0.057	0.099	0.0656
Hg^{201}	0.015	0.057	0.072	0.0375
Hg^{202}	0.042	0.057	0.099	0.0844
Hg^{204}	0.000	0.057	0.057	0.0194
			0.498	0.284

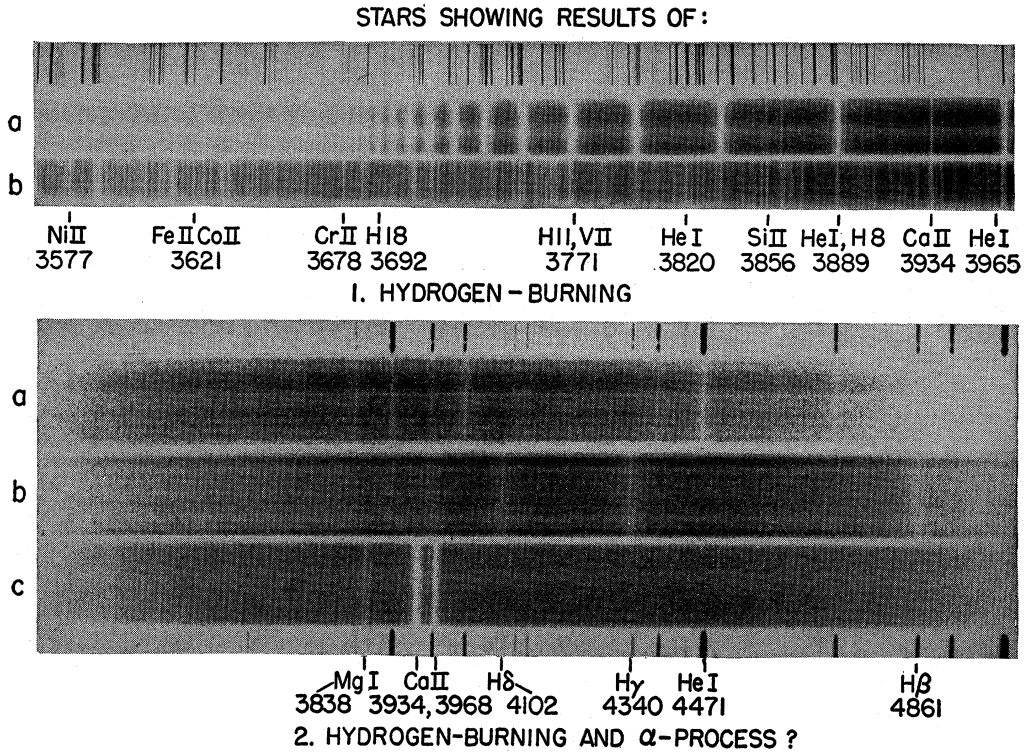

PLATE I.

PLATE 1. Portions of the spectra of stars showing the results of hydrogen burning and possibly the α process. Upper: (a) Normal A-type star, η Leonis, showing strong Balmer lines of hydrogen and a strong Balmer discontinuity at the series limit. (b) Peculiar star, υ Sagittarii, in which hydrogen has a much smaller abundance than normal. Lower: (a) White dwarf, L 1573–31, in which hydrogen is apparently absent. The comparison spectrum above the star is of a helium discharge tube; note the lines of helium in the star's spectrum. (b) White dwarf, L 770–3, which shows broad lines due to hydrogen only, for comparison with (a) and (c). (c) White dwarf, Ross 640, which shows only the two lines due to Ca II and a feature due to Mg I. All the spectrograms in this plate were obtained by J. L. Greenstein; the upper two are McDonald Observatory plates and the lower three are Palomar Observatory plates.

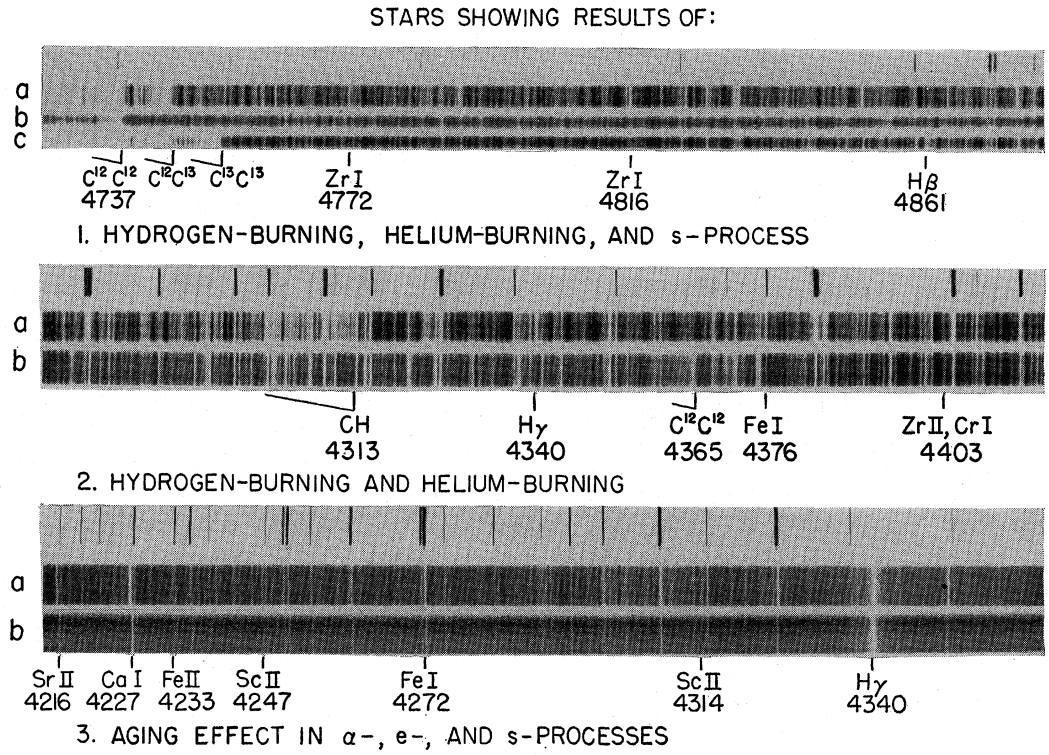

PLATE 2.

PLATE 2. Portions of the spectra of stars showing different aspects of element synthesis. Upper: (a) Normal carbon star, X Cancri, which has $C^{12}/C^{13}\sim3$ or 4. (b) Peculiar carbon star, HD 137613, which shows no C^{13} bands, and in which hydrogen is apparently weak. (c) Normal carbon star, HD 52432, which has $C^{12}/C^{13}\sim3$ or 4. Note that ZrI lines appear to be strongest in (a). Middle: (a) Normal carbon star, HD 156074, showing the CH band and Hγ. (b) Peculiar carbon star, HD 182040, in which CH is not seen, although the weak band of C_2 at λ 4365 is visible. Hγ is also very weak, indicating that hydrogen has a low abundance. Lower: (a) Normal *F*-type star, ξ Pegasi. (b) Peculiar star, HD 19445, which has a slightly lower temperature than ξ Pegasi, yet all lines but hydrogen are much weakened, showing that the abundances of *α*-, *e*-, and *s*-process elements are much lower than normal ("aging" effect). The middle two spectra were obtained by J. L. Greenstein, the remainder, with the exception of HD 137613, by E. M. and G. R. Burbidge.

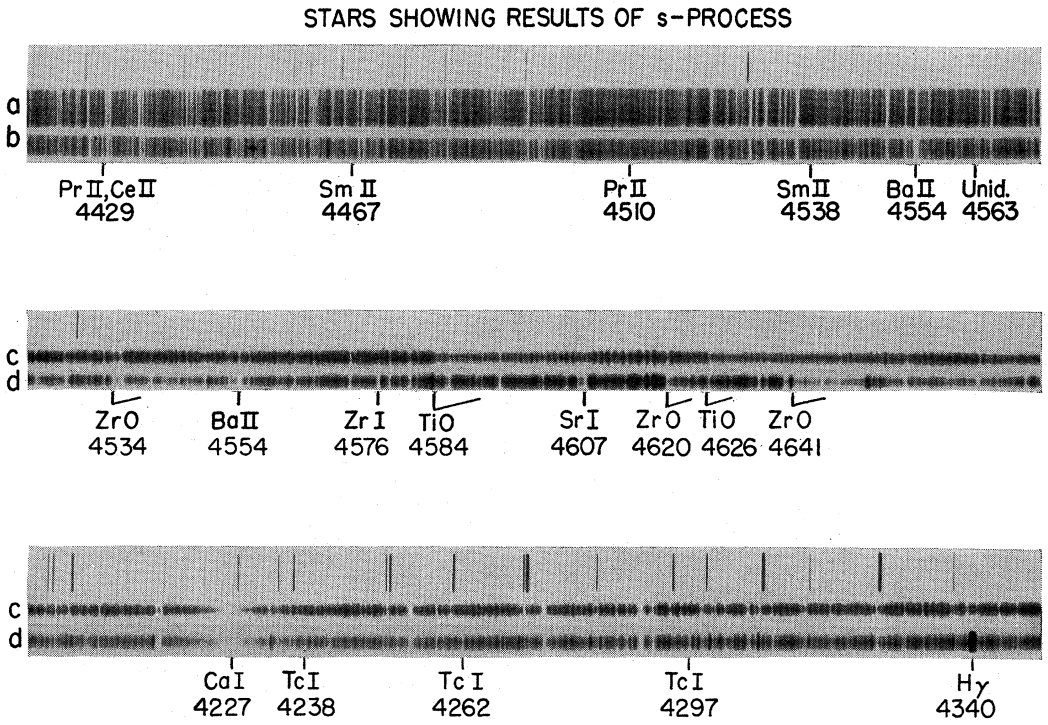

PLATE 3.

PLATE 3. Portions of the spectra of stars showing the results of the *s* process. Upper: (a) Normal *G*-type star, κ Geminorum. (b) Ba II star, HD 46407, showing the strengthening of the lines due to the *s*-process elements barium and some rare earths. Middle: (c) *M*-type star, 56 Leonis, showing TiO bands at λλ 4584 and 4626. (d) *S*-type star, R Andromedae, showing ZrO bands which replace the TiO bands. Lines due to Sr I, Zr I, and Ba II are all strengthened. Lower: (c) Another spectral region of the *M*-type star, 56 Leonis; note that Tc I lines are weak or absent. (d) R Andromedae; note the strong lines of Tc I. The spectrum of R Andromedae was obtained by P. W. Merrill, and the upper two spectra by E. M. and G. R. Burbidge.

Crab Nebula

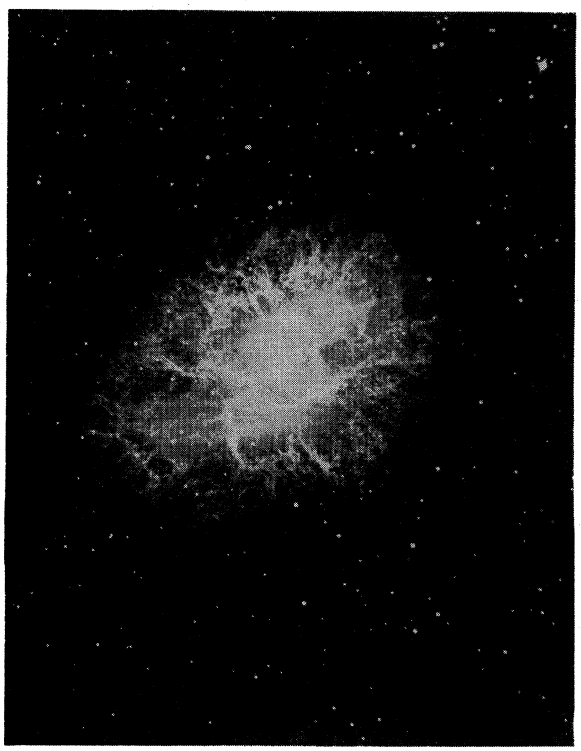

Supernova in IC 4182

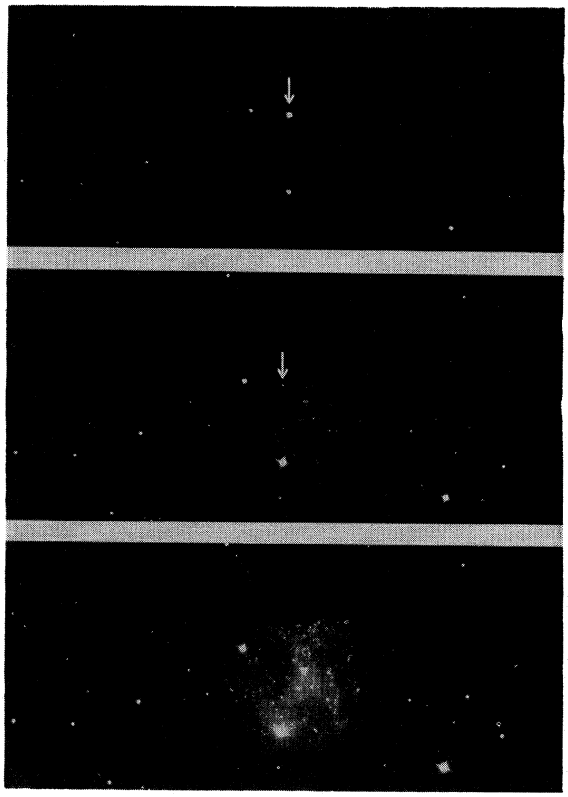

(a)

(b)

(c)

PLATE 4. Left: The Crab Nebula, photographed in the wavelength range λ6300–λ6750. The filamentary structure stands out clearly at this wavelength, which comprises light mainly due to the Hα line. Right: The supernova in IC 4182, photographed (a) September 10, 1937 at maximum brightness—exposure 20 m; (b) November 24, 1938, about 400 days after maximum—exposure 45 m; (c) January 19, 1942, about 1600 days after maximum, when the supernova was too faint to be detected—exposure 85 m. Note that the lengths of the three exposures are different. These plates were taken by W. Baade, to whom we are indebted for permission to reproduce them.